

# The distribution of dark matter in galaxies

Paolo Salucci

Received: date / Accepted: date

**Abstract** The distribution of the non-luminous matter in galaxies of different luminosity and Hubble type is much more than a proof of the existence of dark particles governing the structures of the Universe. Here, we will review the complex but well-ordered scenario of the properties of the dark halos also in relation with those of the baryonic components they host. Moreover, we will present a number of tight and unexpected correlations between selected properties of the dark and the luminous matter. Such entanglement evolves across the varying properties of the luminous component and it seems to unequivocally lead to a dark particle able to interact with the Standard Model particles over cosmological times. This review will also focus on whether we need a paradigm shift, from pure collisionless dark particles emerging from “first principles”, to particles that we can discover only by looking to how they have designed the structure of the galaxies.

**Keywords** Dark matter · Galaxies · Cosmology · Elementary particles

---

**Contents**

1	Introduction . . . . .	3
1.1	Scope of the review . . . . .	3
1.2	The presence of dark matter in galaxies . . . . .	5
2	The invisible character, dark particles and co. . . . .	6
2.1	Collisionless and cold dark particles . . . . .	7
2.2	An unexpected new candidate for cold dark particles . . . . .	8
2.3	Self-interacting DM particles . . . . .	9
2.4	FUZZY dark particles . . . . .	9
2.5	Warm dark matter particles . . . . .	10
2.6	In search for dark matter . . . . .	11
3	Baryons in galaxies . . . . .	12
3.1	Spirals, LSB and UDG . . . . .	12
3.1.1	HI distribution in disk systems . . . . .	13
3.2	Ellipticals . . . . .	13
3.3	Dwarf spheroids . . . . .	14
4	Probing the gravitational potential in galaxies . . . . .	14
4.1	Rotation curves . . . . .	14
4.2	A reference velocity for disk systems . . . . .	16
4.3	Vertical motions . . . . .	16
4.4	Dispersion velocities . . . . .	16
4.5	Fast spheroidal rotators . . . . .	18
4.6	Dispersion velocities versus rotation curves . . . . .	18
4.7	Masses in spheroids within half-light radii . . . . .	18
4.8	Tracer mass estimator . . . . .	19
4.9	Weak lensing . . . . .	19
4.10	Strong lensing . . . . .	20
4.11	X-ray emission & hydrostatic equilibrium . . . . .	20
5	The mass of the stellar component in galaxies . . . . .	21
6	DM halo profiles . . . . .	23
7	Kinematics of galaxy systems . . . . .	26
7.1	The Tully–Fisher and the Baryonic Tully–Fisher . . . . .	26
7.2	The Baryonic Tully–Fisher . . . . .	28
7.3	The universal rotation curve and the radial Tully–Fisher . . . . .	29
8	The dark matter distribution in disk systems . . . . .	32
8.1	Dark matter from stacked RCs . . . . .	32
8.2	Dark matter from individual RCs . . . . .	32
8.2.1	The Galaxy . . . . .	36
8.3	Low surface brightness galaxies . . . . .	37
8.4	Dwarf disks . . . . .	39
9	The distribution of matter in spheroids . . . . .	41
9.1	The fundamental plane in ellipticals . . . . .	41
9.2	The dark matter distribution in ellipticals . . . . .	43
9.3	DM in dwarf spheroidals . . . . .	49
10	The LM/DM universal properties . . . . .	51
10.1	The cored distributions of dark matter halos around galaxies . . . . .	52
10.2	The dark-luminous matter coupling 2.0 . . . . .	54
11	Conclusions . . . . .	55
12	Future directions . . . . .	56

## 1 Introduction

The idea of the presence of large amounts of invisible matter in and around spirals, distributed differently from the stellar and gaseous disks, turned up in the 1970s (Roberts 1978; Faber and Gallagher 1979; Rubin et al. 1980; Bosma 1981a, see also Bertone and Hooper 2016). There were, in fact, published optical and 21-cm rotation curves (RCs) behaving in a strongly anomalous way. These curves were incompatible with the Keplerian fall-off we would predict from their outer distribution of luminous matter (see Fig. 1).

From there, this dark component has started to take a role always more important in cosmology, astrophysics and elementary particles physics. On the other hand, the nature and the cosmological history of such dark component has always become more mysterious and difficult to be derived from paradigms and first principles. We must remark that a dark massive component in the mass budget of the Universe is necessary to explain: the redshift dependence of the expansion of its scale factor, the relative heights of the peaks in the CMB cosmic fluctuations, the bottom-up growth of the cosmological structures to their nonlinear phases, the large scale distribution of galaxies and the internal mass distribution of the biggest structures of the Universe. These theoretical issues and observational evidences (that will not be treated in this review) add phenomenal support to the paradigm of a massive dark particle, which, *a fortiori*, must lay beyond the zoo of the Standard Model of the elementary particles. This support is not able, however, to determine the kind, the nature and the mass of such a particle.

There is no doubt that dark matter connects, as no other issue, the different fields of study of cosmology, particle physics and astrophysics. In the current  $\Lambda$  cold dark matter ( $\Lambda$ CDM) paradigm, the DM is non-relativistic since its decoupling time and can be described by a collisionless fluid, whose particles interact only gravitationally and very weakly with the Standard Model particles (Jungman and al. 1996; Bertone 2010).

In the past 30 years, in the preferred  $\Lambda$ CDM scenario, the complementary approach of detecting messengers of the dark particle and creating it at colliders has brought over an extraordinary theoretical and experimental effort that, however, has not reached a positive result. Moreover, on the scales  $< 50$  kpc, where great part of the DM resides, there is a growing evidence of increasingly quizzical properties of the latter are, so that, a complex and surprising scenario, of very difficult understanding, is emerging.

### 1.1 Scope of the review

The distribution of matter in galaxies does not seem to be the final act of a simple and well understood history which has developed itself over the whole age of the Universe. It seems, instead, to lead to one of the two following possibilities: 1) the dark particle is a WIMP, however, baryons enter, heavily and in a very tuned way, into the process of galaxy formation, modifying,

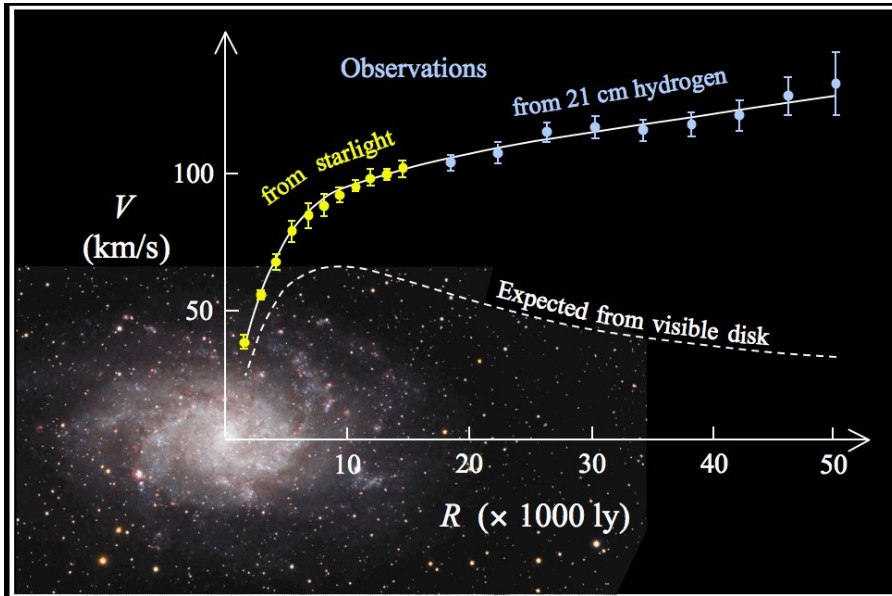


**Fig. 1** The image of M33 and the corresponding rotation curve (Corbelli and Salucci 2000). What exactly does this large anomaly of the gravitational field indicate? The presence of *i*) a (new) non-luminous massive component around the stellar disk or *ii*) new physics of a (new) dark constituent?

rather than following, the original DM distribution 2) the dark particle is something else, likely interacting with SM particle(s) and very likely lying beyond our current ideas of physics.

In both cases, investigating deeply the distribution of dark matter in galaxies is necessary and worthwhile. In the first case, the peculiar imprint that baryons leave on the original distribution of the dark particles can serve us as an indirect, but telling, investigation of the latter. In the second case, with no guidance from first principles, a most complete investigation of the dark matter distribution in galaxies is essential to grasp its nature.

In any case, it is now possible to investigate such issue in galaxies of various morphological types and luminosities. We are sure that this will help us to shed light on the unknown physics underlying the dark matter mystery.

There are no doubts that the topic of this review is related and, in some case, even entangled with other main topics of cosmology and astroparticle physics. However, this work will be kept focused on the properties of dark matter where it mostly resides. Then, a number of issues, yet linked to the dark matter in galaxies, will not be dealt here or will be dealt in a very schematic way. This, both because we sense that looking for the “naked truth” of the galactic dark matter is the best way to approach the related mystery and because there are recent excellent reviews, suitable to complete the whole picture of dark matter in galaxies. These include: “The Standard Cosmological Model: Achievements and Issues” (Ellis et al. 2018), standard and exotic dark-matter

candidate particles and their related searches and productions (Roszkowski et al. 2017; Lisanti 2017), the  $\Lambda$ CDM scenario and its observational challenges (Naab and Ostriker 2017; Somerville and Dave 2015; Bullock and Boylan-Kolchin 2017; Turner 2018), “The Connection Between Galaxies and Their Dark Matter Halos” (Wechsler and Tinker 2018), “Status of dark matter in the universe” (Freese 2017), “Galaxy Disks” (van der Kruit and Freeman 2011) and “Chemical Evolution of Galaxies” (Matteucci 2012). In addition, in the next sections, when needed, I will indicate the readers the papers that extend and deepen the content here presented.

Let us stress that, although in this review one can find several observational evidences that can be played in disfavor of the  $\Lambda$ CDM scenario, this review is not meant to be a collection of observational challenges to such scenario and several issues at such regard, e.g., Muller et al. (2018), will not be considered here.

It is worth pointing out that here we do not consider the theories alternative to the DM, that is, theories that dispose of the dark particle. The main reasons are 1) space: an honest account of them will require to add many more pages to this longish review and 2) my personal bias: no success in explaining the observations at galactic scale can compensate the intrinsic inability that these theories have in conceiving the galaxy formation process and interpreting the *corpus* of the cosmological observations.

## 1.2 The presence of dark matter in galaxies

Let us introduce the “phenomenon” of dark matter in galaxies as it follows: be  $M(r)$  the mass distribution of the gravitating matter and  $M_L(r)$  that of the sum of all the luminous components. Let us notice that the radial logarithmic derivative of both mass profiles can be obtained from observations. Then, we realize that in spirals, for  $r > r_T$ , they do not match, in detail:  $d \log M/d \log r > d \log M_L/d \log r$  (see Fig. 1 where the transition radius  $r_T \simeq 4$  kpc). Then, we introduce a non luminous component whose mass profile  $M_H(r)$  accounts for the disagreement:

$$\frac{d \log M(r)}{d \log r} = \frac{M_L(r)}{M(r)} \frac{d \log M_L}{d \log r} + \frac{M_H(r)}{M(r)} \frac{d \log M_H}{d \log r}. \quad (1)$$

The above immediately shows that the phenomenon of the mass discrepancy in galaxies emerges from the discordance between the value of the radial logarithmic derivative of the total mass profile and that of the luminous mass profile. We need to insert in the r.h.s. of Eq. (1) an additional (dark) term. This also implies that the DM phenomenon emerges observationally and can be investigated only if we are able to accurately measure the distribution of luminous and gravitating matter. In fact, the rotation curves  $V(r) \propto (M(r)/r)^{1/2}$  have a property which is rarely found in astrophysics. We start with the fact that a good determination of the logarithmic derivative  $\nabla \equiv d \log V/d \log r$

is essential to successfully mass model a galaxy. Now, the analysis of  $N$  individual RCs with the same value of  $\nabla = \nabla_0$  and with a large uncertainty, e.g.,  $\delta\nabla_0 = 0.2$  gives much *less* information on the mass distribution than one single RC with  $\delta\nabla_0 = \pm 0.2/\sqrt{N}$ . In short a RC with large uncertainties gives no information on the underlying galaxy mass distribution.

There is, however, a way to exploit the information carried by the low quality RCs, namely, to properly *stack* them in coadded curves, killing so large part of their random uncertainties.

The luminous components of galaxies show a striking variety in morphology and in the values of their structural quantities. The range in magnitudes and central surface brightness are 15 mag and 16 mag/arcsec<sup>2</sup>. The distribution of the luminous matter in spirals is given by a stellar disk + a stellar central bulge and an extended HI disk and in ellipticals and dSphs by a stellar spheroid.

How will the variety of the properties of the luminous matter contrast with the organized uniformity of the dark matter? The phenomenological scenario of dark matter in galaxies that we discuss in this review has to be considered as a privileged way to understand what dark matter halos are made of and to approach the involved (new) laws or processes of Nature.

Freeman (1970), in its Appendix A, firstly drew the attention of the astrophysical community to a discrepancy between the kinematics and the photometry of the spiral galaxy NGC 300, that implied the presence of large amounts of non-luminous matter. Then, during the 1970s the contribution of Morton Roberts to the cause of DM in galaxies has been crucial (Bullock and Boylan-Kolchin 2017). A next topical moment was when Vera Rubin published 20 optical RCs extended out to well beyond the optical radii  $R_{\text{opt}}$  that were still rising or flattish at the last measured point (Rubin et al. 1980) and similar decisive kinematics was obtained by means of several 21-cm rotation curves extended out to the optical radii (Bosma 1981a,b). Moreover, we have to mention the Faber and Gallagher (1979) review that played a very important role to spread the idea of a dark halo component in galaxies.<sup>1</sup>

In this brief historical account of the discovery of dark matter in galaxies, one point should still be made. Until to few years ago, the nature of dark matter was not meant to be determined by the properties of the galaxy gravitational field, but to come from first principles verified by large scales observations. In this review, instead, we will follow also a reverse-engineering approach: the unknown nature of the DM is searched within the (complex) observational properties of the dark halos in galaxies.

## 2 The invisible character, dark particles and co.

It is worth starting this review with a brief account of the dark matter candidate particles presently in the ballpark; one has to keep on mind however, that there are likely to risk not to be “the” DM particle.

<sup>1</sup> Only much later the universality of the DM phenomenon in spirals did emerge (Persic, Salucci and Stel 1996).

## 2.1 Collisionless and cold dark particles

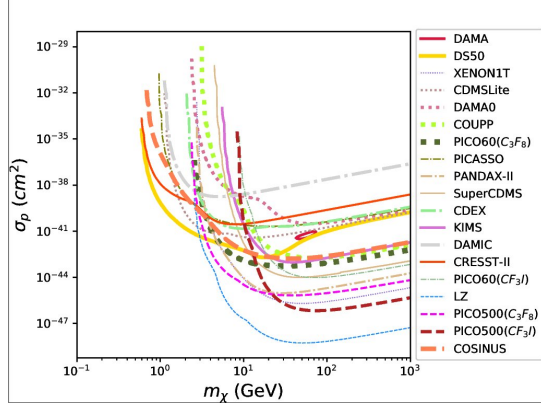


**Fig. 2 top** Current 90% C.L. exclusion plots to the effective WIMP–proton cross section, see Kang et al. (2018).

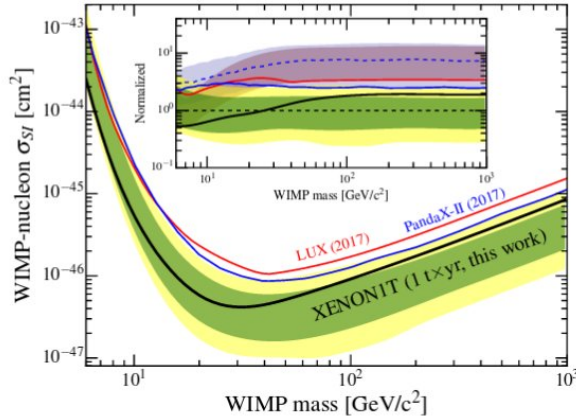


**Fig. 3** Current 90% C.L. exclusion plots to the effective WIMP–nucleon cross section. Image reproduced with permission from Aprile et al. (2018), copyright by APS.

Let us start by recalling the motivations that have led to about 30 years of fascination with the Weakly-Interacting Massive Particles (WIMPs) and especially with the lightest supersymmetric particle (Steigman and Turner 1985, see also Kolb and Turner 1990). At high temperatures, ( $T \gg m_{\text{WIMP}}$ ), WIMPs are thermally created and destroyed. As the temperature of the Universe decreases due to its expansion, the density is exponentially suppressed

( $\propto \exp[-m_{\text{WIMP}}/T]$ ) and becomes no longer high enough to pair-create them. When the WIMP mean free path is comparable to the Hubble distance, the particles also cease to annihilate, leave the thermal equilibrium state and “freeze-out”. At this point, the co-moving density remains constant. The temperature for which the freeze-out occurs is about 5% of the WIMP mass. Therefore, the (relic) density becomes constant when the particles are non-relativistic. The value of the relic density  $\Omega_{\text{WIMP}}$  depends only on the total annihilation cross-section  $\sigma_A$  and the particles’ relative velocity  $|\mathbf{v}|$ :

$$\Omega_{\text{WIMP}} \simeq \frac{6 \cdot 10^{-27} \text{ cm}^3 \text{ s}^{-1}}{\langle \sigma_A |\mathbf{v}| \rangle}, \quad (2)$$

The scale of weak interaction strength ( $\sim \alpha^2/m_{\text{WIMP}}^2$ ) implies that  $\langle \sigma_A |\mathbf{v}| \rangle > 10^{-25} \text{ cm}^3 \text{ s}^{-1}$ , where  $\sigma_A$  is the cross section and the WIMP mass is taken to be 100 GeV. The resulting relic density for such a particle would be within a factor 3 of the measured value of the dark matter density  $\Omega_m$  (e.g., Planck Collaboration et al. 2016). This remarkable coincidence is referred to as the “WIMP miracle.” This particle, today, should interact with ordinary matter only through weak interaction, in addition to the gravitational one. The former should occur via the exchange of a scalar particle, or a vector boson interaction. These interactions together with the particle-particle annihilations ongoing in the densest region of the Universe, would make the particle detectable.

It is known that this scenario reproduces a wealth of cosmological observations, particularly on scales  $> 10$  Mpc. On the other hand, WIMPs have so far escaped detection (see Figs. 2–3) and, furthermore, there is a number of small-scale issues that put in question their being the dark particle in galaxies.

## 2.2 An unexpected new candidate for cold dark particles

There might be a connection between the dark matter in galaxies, in particular the cold DM and the gravitational waves produced by the merging of stellar-mass black holes and possibly detectable by LIGO-Virgo experiments. This is due to the intriguing possibility that DM consists of black holes created in the very early Universe. In this case, the detection of primordial black hole binaries could provide an unambiguous observational window to pin down the nature of dark matter (Green 2016). These objects are also detectable as effect of their continuous merging since recombination. This violent process can have generated a stochastic background of gravitational waves that could be detected by LISA and PTA (see also García-Bellido (2017)).

It is known that massive primordial black holes form at rest with respect to the flow of the expanding Universe and then with zero spin. Moreover, they have negligible cross-section with the ordinary matter and constitute a right candidate for the  $\Lambda$ CDM scenario (see, however, Koushiappas and Loeb 2017). Of course, just substituting WIMPs with primordial BHs does not immediately relieve the severe tension with the observations at galactic scales that these particles have. It is, however open the question whether these primordial BHs



could have some sort of interaction with baryons which is instead forbidden to WIMPs.

### 2.3 Self-interacting DM particles

Self-interacting dark matter (SIDM) particles were proposed by Spergel and Steinhardt (2000) (see also Boddy et al. 2014; Bode et al. 2004) to solve the core-cusp and missing satellites problems (see also Tulin and Yu 2017; Bellazzini et al. 2013). DM particles scatter elastically with each other through 2-2 interactions and, as low-entropy particles, are heated by elastic collisions within the dense inner halo and leave the region: the central and nearby densities are then reduced, turning an original cusp into a core. The collision rate is:

$$R_{\text{scatt}} = \sigma v_{\text{rel}} \rho_{\text{DM}}/m \approx 0.1 \text{ Gyr}^{-1} \times \left( \frac{\rho_{\text{DM}}}{0.1 M_{\odot}/\text{pc}^3} \right) \left( \frac{v_{\text{rel}}}{50 \text{ km/s}} \right) \left( \frac{\sigma/m}{1 \text{ cm}^2/\text{g}} \right), \quad (3)$$

where  $m$  is the DM particle mass,  $\sigma, v_{\text{rel}}$  are the cross section and relative velocity for scattering. Within the central region of a typical dwarf galaxy we have:  $\rho_{\text{DM}} \sim 0.1 M_{\odot}/\text{pc}^3$  and  $v_{\text{rel}} \sim 50 \text{ km/s}$ . Therefore, the cross section per unit mass ( $\sigma/m$ ) must be at least:

$$\sigma/m \sim 1 \text{ cm}^2/\text{g} \approx 2 \times 10^{-24} \text{ cm}^2/\text{GeV} \quad (4)$$

to have an effect; this corresponds to about one scattering per particle over 10 Gyr galactic timescales. With the above value of  $\sigma/m$ ,  $R_{\text{scatt}}$  is negligible during the early Universe when structures form. SIDM, therefore retains the success of large-scale structure formation of the  $\Lambda$ CDM scenario, and affects the dark structures on small scales only once they are already virialized.

The self-interacting dark matter is then a cusp-core density profile transformer (e.g., Vogelsberger et al. 2014; Zavala et al. 2013; Kaplinghat et al. 2015). As result of the annihilation among these particles in the denser inner regions of the galactic halos, the originally cuspy DM density becomes constant with radius. Outside the core region, the number of annihilations rapidly falls as  $\rho_{\text{DM}}^2(r)$  and the halo profile remains identical to the original one.

### 2.4 FUZZY dark particles

The idea is that the dark matter is a scalar dark particle of mass  $m_a \sim 10^{-22} \text{ eV}$ . At large scales its coherent macroscopic excitations can mimic the behavior of the cold dark matter (CDM). At the scale of galaxies, however, this particle has macroscopic wave-like properties that may explain the classic “discrepancies” of the standard DM scenario (Weinberg 1977; Hui et al. 2016; Bernal et al. 2017; Ringwald 2012).

Once in galaxies, these particles behave as Bose–Einstein condensate (BEC); in this model, the inter-particle distance is much smaller than their de Broglie

wave length. The particles move collectively as a wave: their equation of state can lead to cored configuration like those observed. The capability to detect such Bose–Einstein-condensed scalar field dark matter with the LIGO experiment is under analysis (Li et al. 2017).

## 2.5 Warm dark matter particles

Warm dark matter (WDM) particle decouples from the cosmological plasma when it is still mildly relativistic. These particles can be created in the early Universe in a variety of ways (Dodelson and Widrow 1994; Shi and Fuller 1999; Kusenko 2009). In the case where the WDM consists of thermal relics, the suppression of small-scale power in the linear power spectrum (e.g., Bringmann et al. 2016)  $P_{\text{WDM}}$ , can be conveniently parametrized by reference to the CDM power spectrum  $P_{\text{CDM}}$ , see Fig. 4. In the more likely cases in which the WDM particle is a non-resonantly produced sterile neutrino, its mass  $m_{\text{sterile}}$ , can be related to the mass of the equivalent thermal relic (Viel et al. 2005). This conversion depends on the specific particle production mechanism.

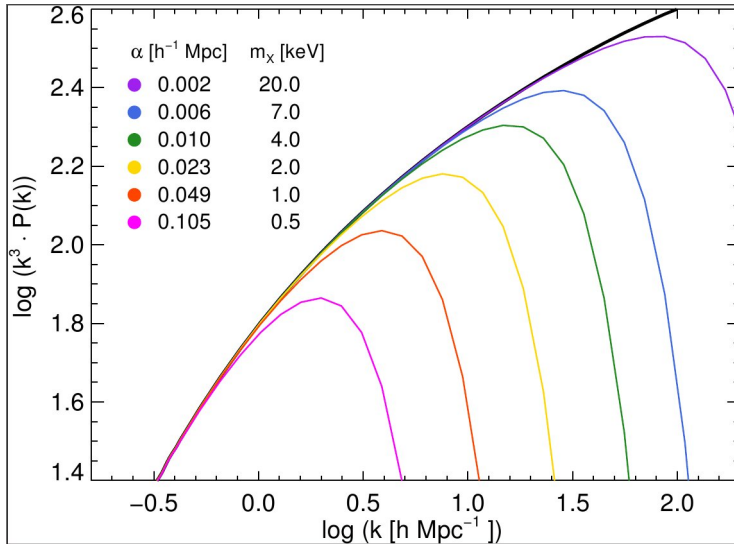


**Fig. 4** Linear power spectra in  $\Lambda$ CDM (*black line*) and  $\Lambda$ WDM (*coloured lines*) scenarios.  $\Lambda$ WDM models are labelled by their thermal relic mass and value of the damping scale  $\alpha$ . We have  $(\frac{P_{\text{WDM}}}{P_{\text{CDM}}})^{1/2} = [1 + (\alpha k)^{2/1.1}]^{-5/1.1}$ ,  $k$  is the wave-number. Image reproduced with permission from Kennedy et al. (2014), copyright by the authors.

Given the mass of this particle being about 2 keV, its de Broglie length-scale is of the order of 30 kpc, so that, inside the optical region of galaxies a quantum pressure emerges (Destri et al. 2013; de Vega and Sanchez 2017) and plays a role in the equilibrium of the structures. The DM particles follow,

then, a Fermi–Dirac distribution:

$$f_{\text{FD}}(p; T, \mu) = \frac{g}{(2\pi\hbar)^3} \frac{1}{\exp[(E - \mu)/T] + 1}, \quad (5)$$

where  $p$  and  $E = p^2/(2m)$  are the momentum and the single-particle kinetic energy;  $T(r)$ , expressed in terms of energy, is the average temperature of DM particles at a radius  $r$ :  $T(r) \propto V^2(r)$  in spirals and  $T(r) \propto \sigma_{\text{l.o.s.}}^2(r)$  in pressure dominated systems. Noticeably,  $f(p)$  has an upper limit:  $f(p) \leq \frac{g}{(2\pi\hbar)^3}$ , where  $g$  is the number of internal degrees of freedom. We have, in this case, that the quantum pressure and not the Gravity Force shapes the inner DM density profile. WDM particles can be detected: they can produce a monochromatic gamma ray line at  $2m_{\text{WDM}}$  keV, which is constrained by X-ray measurements, e.g., Boyarsky et al. 2007.

The properties of WDM particles, their scientific case and cosmological role and the various strategies to detect them, have recently been presented in a White Paper (Adhikari et al. 2017).

## 2.6 In search for dark matter

For 30 years, WIMPs have been the first target in our attempt to detect and identify the dark particle. During the past decades, the sensitivity of the experiments involved has improved by three to four orders of magnitude, but an evidence for their existence is yet to come. On the other hand, searches at hadron colliders (which attempts to produce WIMPs through the collision of high energy protons and the subsequent formation of stable dark matter particles that can be identified through the production of quarks and gluons), have given no result (see Butler 2018).

It is agreed that no conclusive detection signal of the particle has yet arrived as result of a many year-long extensive search program that combined, in a complementary way, direct, indirect, and collider probes (see Arcadi et al. 2017 for a detailed review).

However, it is worth discussing astrophysical aspects, related to the above searches, that have an intrinsic importance and that are valid also for any particle investigation. In direct searches, the differential event rate  $R_{\text{scatt}}$

$$\frac{dR_{\text{scatt}}}{dE} \propto g(v_{\text{min}})\rho(R_{\odot}), \quad (6)$$

is proportional to  $\rho(R_{\odot})$  the local (i.e., at the solar radius) dark matter density and to the function  $g(v_{\text{min}}) = \int_{v > v_{\text{min}}}^{v_{\text{esc}}} \frac{f(\mathbf{v})}{v} d^3\mathbf{v}$ .  $v_{\text{min}}$  is the minimum particle speed that can cause in the detector a recoil of energy  $E$  (Gondolo 2002).

$v_{\text{esc}}$  is the escape velocity from the Milky Way:  $v_{\text{esc}} = (570 \pm 120)\text{km/s}$  (Nesti and Salucci 2013). A reference value of  $\rho(R_{\odot}) = 0.3 \text{ GeV/cm}^3$  is often adopted however recent accurate determinations indicate a rather higher value:  $\rho(R_{\odot}) = (0.43 \pm 0.06) \text{ GeV/cm}^3$  (Salucci et al 2010; Catena and Ullio 2010).

To obtain  $g(v_{\min})$ , one needs the whole DM density distribution, however, for the Milky Way, we can consider the galaxy halo as an isotropic isothermal sphere with density profile  $\rho(r) \propto r^{-2}$ . Then  $f(\mathbf{v}) = \frac{N}{2\pi\sigma_v^2} \exp\left(-\frac{\mathbf{v}^2}{2\sigma_v^2}\right)$ , where  $N$  is a normalization constant and  $\sigma_v$  is the DM particles one-dimensional velocity dispersion, which in the present model is related to the circular velocity  $V(r)$  by:  $\sigma_v = V(r)/\sqrt{2}$ .

The indirect searches of DM are based on astrophysical observations of the products of the DM particles self-annihilation (or decay) able to climb up the emissions coming from the likely astrophysical mechanisms also producing antiprotons and positrons. The photon spectrum  $\frac{dN_\gamma^f}{dE_\gamma}$ , with  $E_\gamma$  the photon energy, is expected to be proportional to  $\int_{1.o.s.} dl \rho^2(r)$  for annihilations and  $\int_{1.o.s.} dl \rho(r)$  for decays; as usual,  $\rho(r)$  is the DM density within the galaxy and the integrals are performed over the line of sight  $l$ . The dependence of  $\rho(r)$  on the above fluxes leads to a dependence of the signal on the inner distribution of DM in galaxies, modulo the fraction between the size of the dark halo and that of the telescope beam both projected on the plane of the sky (for details including the application to the Galactic Center, see Gammaldi 2016). As consequence of that, indirect searches require an accurate knowledge of the halo density profiles and, in this perspective, one should also consider cored dark matter halo distributions, in performing the analysis on the  $\gamma$  flux. Here, we do not further enter in this (important) issue (see, e.g., Gammaldi 2016).

### 3 Baryons in galaxies

The luminous components in galaxies show a striking variety in morphology and in dimensions. Noticeably, the total luminosity and the radius  $R_{1/2}$  enclosing half of the latter are good tags of the objects.

#### 3.1 Spirals, LSB and UDG

Caveat some occasional cases not relevant for the present topic, the stars are distributed in a thin disk with surface luminosity (Freeman 1970, for a study on 967 late type spirals, see Persic, Salucci and Stel 1996)

$$I(R) = I_0 e^{-R/R_D} = \frac{M_D}{2\pi R_D^2} e^{-R/R_D} \left(\frac{M_D}{L}\right)^{-1}, \quad (7)$$

where  $R_D = 1/1.67 R_{1/2}$  is the disk length scale,  $I_0$  is the central value of the surface luminosity and  $M_D$  is the disk mass. The light profile of late spirals does not depend on galaxy luminosity and the length scale  $R_D$  sets a consistent reference spatial scale.<sup>2</sup>

<sup>2</sup> We take  $R_{\text{opt}} \equiv 3.2 R_D$  as the reference stellar disk edge.

The contribution to the circular velocity from this stellar component is:

$$V_{\text{disk}}^2(r) = \frac{GM_D}{2R_D} x^2 B\left(\frac{x}{2}\right), \quad (8)$$

where  $x \equiv R/R_D$  and  $B = I_0 K_0 - I_1 K_1$ , a combination of known Bessel functions.

Classical LSB galaxies usually have central surface brightness down to  $\mu_B(0) \sim 22\text{--}23$  mag arcsec $^{-2}$  (Impey et al. 1988). Extremely low surface brightness (LSB) galaxies with unexpectedly large sizes, namely ultra-diffuse galaxies (UDGs), are found in nearby galaxy clusters (Bothun et al. 1991; Toloba et al. 2018). UDGs have much lower central surface brightness ( $\mu(0) = 24\text{--}26$  mag arcsec $^{-2}$  in  $g$  band and half-light radii  $R_{1/2} > 1.5$  kpc that, in spirals, are found in objects with stellar masses more than 10 times higher (van Dokkum et al. 2015; Shi et al. 2017). In LSBs/UDGs the stellar disks follow the Freeman exponential profile as in normal spirals, but their two structural parameters ( $I_0$  and  $R_D$ ) do not correlate as in the latter, where, approximately:  $L_I \propto R_D^2$ .

### 3.1.1 HI distribution in disk systems

Spirals have a gaseous HI disk which usually is important only as tracer of the galaxy gravitational field. Only at the outer radii ( $R > R_{\text{opt}}$ ) of low luminosity objects, such disk becomes the major baryonic component of the circular velocity and must be included in the galaxy velocity model.

The HI disks show, very approximately, a Freeman distribution with a scale length about three times larger than that of the stellar disc (Evoli et al. 2011; Wang et al. 2014).

$$\mu_{\text{HI}}(R) = \mu_{\text{HI},0} e^{-\frac{R}{3R_D}} \quad (9)$$

A rough estimate of the contribution of the gaseous disc to the circular velocity is

$$V_{\text{HI}}(R)^2 = 1.3 \left(\frac{M_{\text{HI}}}{9M_D}\right) V_{\text{disk}}^2\left(\frac{R}{3R_D}\right) \quad (10)$$

where the coefficient 1.3 is due to the He contribution. Of course when the resolved HI surface density is available, one derives  $V_{\text{HI}}(R)^2$  directly from the latter. Inner H $_2$  and CO disks are also present, but they are negligible with respect to the stellar and HI ones (Gratier et al. 2010; Corbelli and Salucci 2000).

## 3.2 Ellipticals

Ellipticals are more compact objects than spirals so that, in objects with same stellar mass  $M_*$ , they probe inner regions of the DM halo than spirals. Their profiles are well represented by the Sersic Law:

$$\ln \left[ \frac{\Sigma_S(R)}{\Sigma_{R_e}} \right] = -q \left[ \left( \frac{R}{R_e} \right)^{\frac{1}{m}} - 1 \right], \quad (11)$$

$\Sigma_S(0) = \Sigma_{R_e} e^q$ , where  $R$  is the projected radial coordinate in the plane of the sky,  $\Sigma_{R_e}$  is the line of sight (l.o.s.) projected surface brightness at a projected scale radius  $R_e \simeq R_{1/2}$  and  $q = 2m - 1/3$  with  $m$  a free parameter. By deprojecting the surface density  $\Sigma_S(R/R_e, m)$ , we obtain the luminosity density  $j(r)$  and by assuming a radially constant stellar mass-to-light ratio  $(M/L)_*$  we obtain the spheroid stellar density  $\rho_*(r)$ .

### 3.3 Dwarf spheroids

The distribution of stars in dSph plays a major role in the analysis of their internal kinematics. The information we have comes from the bright stars detected by dedicated imaging or spectroscopy and, more recently, by surveys like the Sloan Sky Digital Survey and Gaia. The 3D stellar density is obtained from the deprojection of the 2D luminosity profile and an assumed mass-to-light ratio. The former is well reproduced by the Plummer density profile (Plummer 1915), characterized by a length scale  $R_e$  and a central density  $\nu_0 = 3 M_{\text{sph}} / (4\pi R_e^3)$  with  $M_{\text{sph}}$  the total stellar mass. The projected mass (luminosity) distribution is given by:  $\Sigma(R) = \frac{M_{\text{sph}}}{\pi R_e^2} (1 + x^2)^{-2}$ ,  $x = R/R_e$ . Then, the 3D stellar density is given by

$$\nu(x) = \nu_0 (1 + x^2)^{-5/2}. \quad (12)$$

## 4 Probing the gravitational potential in galaxies

### 4.1 Rotation curves

The rotation curves (RCs) of spirals are an accurate proxy of their gravitational potential. We measure recessional velocities by Doppler shifts, and from these (often 2D) data, we construct the RC  $V(R)$ . This process estimates also the sky coordinates of the galaxy kinematical center, its systemic velocity, the degree of symmetry and, often, the inclination angle.

Notice that the effectiveness of the RC is proved in many ways: e.g., in systems with  $M_I < -18$  in the innermost luminous matter dominated regions the gravitating mass (measured by  $V(R)$ ) agrees with the predictions from the light distribution (Ratnam and Salucci 2000).

The rotation curves in disk systems have 3 different components: the relationship with the total gravitational potentials  $\phi_{\text{tot}} = \phi_b + \phi_H + \phi_{\text{disk}} + \phi_{\text{HI}}$  is

$$V_{\text{tot}}^2(r) = r \frac{d}{dr} \phi_{\text{tot}} = V_b^2 + V_H^2 + V_{\text{disk}}^2 + V_{\text{HI}}^2. \quad (13)$$

Then, the velocity fields  $V_i$  are the solutions of the four separated equations:  $\nabla^2 \Phi_i = 4\pi G \rho_i$  where  $\rho_i$  are dark matter, stellar disk, stellar bulge, HI disk surface/volume densities ( $\rho_h(r)$ ,  $\rho_{bu}(r)$ ,  $\mu_d(r)\delta(z)$ ,  $\mu_{\text{HI}}(r)\delta(z)$  with  $\delta(z)$  the Kronecker function,  $z$  the cylindrical coordinate) and  $\phi_i$  the gravitational potential.

Recently, a new way to exploit the RC to obtain the DM halo density distribution has been devised (Salucci et al 2010). We assume that spirals are composed by a stellar disk (Freeman 1970), a HI disk and an unspecified spherical DM halo with density profile  $\rho_H(r)$ . Other baryonic components can be added, if needed.<sup>3</sup> From the radial derivative of the equation of centrifugal equilibrium we obtain

$$\rho_H(r) = \frac{1}{4\pi Gr^2} \frac{d}{dr} \left[ r^2 \left( \frac{V^2(r)}{r} - a_D(r) \right) \right], \quad (14)$$

We have  $a_D(r) = \frac{GM_D r}{R_D^3} (I_0 K_0 - I_1 K_1)$ , where  $I_n$  and  $K_n$  are the modified Bessel functions computed at  $\frac{r}{2R_D}$ . Noticeably, the second term of the r.h.s. of Eq. (14) goes exponentially to zero for  $r/R_D > 2$  (see Fig. 5). Then, for  $R > 2R_D$ , we can determine the DM density profile (see Fig. 5). On the other hand, for  $R < R_D$ , the DM distribution is negligible, so that, if we have a good spatial coverage of the inner RC, we can use Eq. (14) also to obtain the disk mass with good precision.

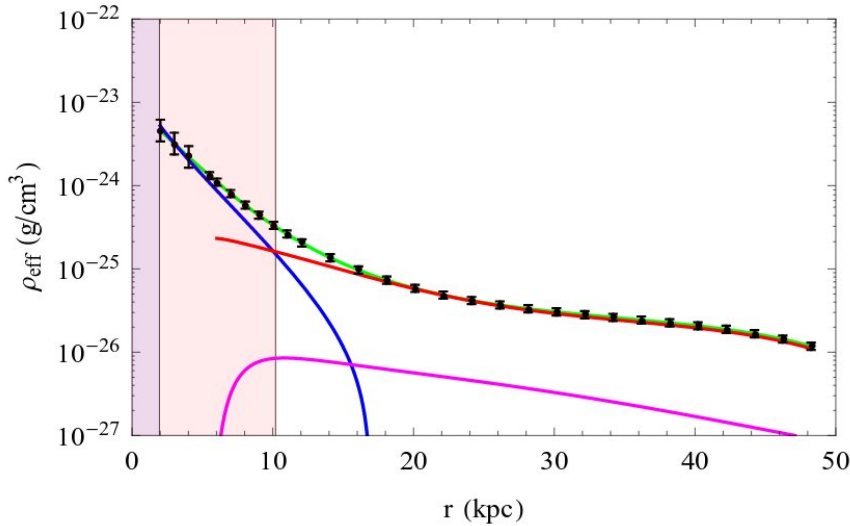


**Fig. 5** A test case: NGC 3198. Effective total density (*points with errorbars*). Contributions: stellar disk (*blue*), HI disk (*magenta*), dark matter (*green line*), all components (*green*). Regions in which the method: 1) is not applicable (*pink*), 2) provides us with a) the value of disk mass (*green*) b) the halo density profile (*white*). Image reproduced with permission from Karukes et al. (2015), copyright by ESO.

<sup>3</sup> The HI component is obtained directly from observations, however, it is always negligible because  $dV_{\text{HI}}^2/dr \simeq 0$ .

## 4.2 A reference velocity for disk systems

In spite of the fact that  $V(R)$ , the circular velocity, is a function of radius we often require a meaningful reference velocity to tag each disk system. In the literature there is no shortage of proposed reference velocities, among those:  $V_{\text{flat}}$ ,  $V_{\text{last}}$ , the linewidths  $W_{20}$ ,  $W_{50}$  and the maximum velocity  $V_{\text{max}}$ . Obviously, if the RC of an object is not available, we are forced to choose one of these kinematical measurements as a reference velocity, however, we must stress that they are very biased: a) a flat part of the RC occurs only a limited number of objects and only over a limited radial region (Persic, Salucci and Stel 1996); b)  $V_{\text{last}}$  depends on the distribution of HI in the galaxies and on the sensitivity of radio telescope used; c) the linewidths are similar to the case b) and furthermore they depend on the full RC profiles; d) the significance of  $V_{\text{max}}$  changes as galaxy luminosity changes, sometimes coinciding with the outermost available velocity, in other cases, with the innermost one. The best unbiased reference velocity for spirals is the quantity:  $V(kR_D)$  that also involves the stellar disks length scale. We have  $k = 2.2$  or  $3.2$ , according whether we are investigating the properties of the luminous or of the dark matter.

## 4.3 Vertical motions

The main goal of the DiskMass Survey (Bershady et al. 2010a,b) was to determine the dynamical mass-to-light ratio of the galaxy disks  $(M/L)_{\text{dyn}}$  by a suitable use of the stellar and gas kinematics. At a radius  $R$ , for a locally isothermal disk, we have

$$(M/L)_{\text{dyn}} = \frac{\sigma_z^2}{\pi G b h_z I(R)}, \quad (15)$$

where the value  $b = 1.5$  is a reasonable approximation for the composite (gas+stars) density distribution (van der Kruit 1988),  $I$  the surface luminosity obtained from the photometry,  $\sigma_z$  the vertical component of the stellar velocity dispersion. Noticeably, with the advent of 2-dimensional spectroscopy using integral field units (IFU), the accuracy and the  $z$ -extension of the measurements of  $\sigma_z$  has been dramatically increased;  $h_z$  is the disk scale height (van der Kruit and Searle 1981; Bahcall 1984) that can be directly measured, and that well correlates with the disk scale length  $R_D$  (Kregel et al. 2002; Bershady et al. 2010a).

Let us stress that this approach leading to Eq. (15) is certainly a new avenue for investigating dark matter in galaxies, but some warning must be raised in that it can be subject to relevant biases (Hessman 2017).

## 4.4 Dispersion velocities

It is well known that in spheroids the kinematics is complex, the stars are in gravitational equilibrium by balancing the gravitational potential, they are



subject to, with the pressure arisen from the r.m.s. of their 3D motions. Moreover, we cannot directly measure the radial/tangential velocity dispersions linked to the mass profile, but only their projected values (e.g., Coccato et al. 2009).

The SAURON (Bacon et al. 2001) Integral Field Spectroscopy survey (de Zeeuw et al. 2002) was the first project to map the two-dimensional stellar kinematics of a sample of 48 nearby ellipticals with  $M_B < 18$ . This survey was followed by the ATLAS<sup>3D</sup> project (Cappellari et al. 2011), a multiwavelength survey of 260 ETGs galaxies. In Cappellari (2016) one finds the details of these observations.

The dispersion velocity is related to the gravitational potential of a galaxy by the Jeans equation that we express as (Binney and Tremaine 2008)

$$\frac{\partial \ln \sigma_r^2}{\partial \ln r} = -\frac{1}{\sigma_r^2} \frac{GM}{r} - \gamma_* - 2\beta. \quad (16)$$

Here,  $G$  is the gravitational constant and  $M(r)$  is the enclosed mass. The velocity anisotropy  $\beta = 1 - \frac{\sigma_\theta^2 + \sigma_\phi^2}{2\sigma_r^2}$ , where  $\sigma_{\theta,\phi,r}$  are the velocity dispersions in the  $r, \theta$  and  $\phi$  directions, can be a function of radius  $r$  (Binney and Tremaine 2008). It is useful to define:  $\alpha = d \log \sigma_r / d \log r$ . Almost always the motions in the  $\theta$  and  $\phi$  directions are assumed to coincide.

$\nu_*$  is the 3D stellar density distribution,  $\gamma_* = d \log \nu_* / d \log r$ . Under the assumption of constant  $\beta$ , the radial velocity dispersion  $\sigma_r(r)$  can be expressed as

$$\sigma_r^2(r) = \frac{1}{\nu_*(r)} \int_r^\infty \nu_*(r') \left(\frac{r'}{r}\right)^{2\beta} \frac{GM(r')}{r'^2} dr'. \quad (17)$$

We can then determine the galaxy mass profile by means of Eq. (17) and the line-of-sight velocity dispersion  $\sigma_{\text{l.o.s.}}$  when the anisotropy factor  $\beta(r)$  is known or assumed:

$$\sigma_{\text{l.o.s.}}^2(R) = \frac{1}{I(R)} \int_{R^2}^\infty dr^2 \frac{\nu_*}{\sqrt{r^2 - R^2}} \sigma_r^2 \left[1 - \beta \frac{R^2}{r^2}\right], \quad (18)$$

where  $I(R)$  and  $\nu_*(r)$  are related by  $I(R) = 2 \int_R^{+\infty} \frac{\nu_*(r)r dr}{\sqrt{r^2 - R^2}}$ .  $I(R)$  and  $\sigma_{\text{l.o.s.}}(R)$  are directly measured.

The Schwarzschild method can be seen as a (complex) extension of the Jeans method and it is especially applied to dSph galaxies where the stellar component is totally negligible (Cretton et al. 1999; Breddels et al. 2013). It is based, fixed a specific gravitational potential, on the integration of test particle orbits drawn from a grid of integrals of motions, i.e., the energy and the angular momentum. The main feature of this method is that, differently from the Jeans method, it can successfully use the observed second and fourth velocity moment profiles to break the mass-anisotropy degeneracy (Breddels et al. 2013).

#### 4.5 Fast spheroidal rotators

In the case of objects (e.g., S0 galaxies) in which the dispersion velocity combine with the rotation motions to balance the galaxy self-gravity, there is a simple and efficient anisotropic generalization of the axisymmetric Jeans formalism which is used to model the stellar kinematics of galaxies (see Cappellari (2016) for details). The following is assumed: (i) a constant mass-to-light ratio  $M/L$  and (ii) a velocity ellipsoid that is aligned with cylindrical coordinates  $(R, z)$  and characterized by the classic anisotropy parameter  $\beta_z = 1 - \sigma_z^2/\sigma_R^2$ . These simple models are fit to integral-field observations of the stellar kinematics of fast-rotator early-type galaxies. With only two free parameters ( $\beta_z$  and the inclination) the models generally provide remarkably good descriptions of the shape of the first ( $V$ ) and second ( $V_{\text{rms}} \equiv \sqrt{V^2 + \sigma^2}$ ) velocity moments. The technique can be used to determine the dynamical mass-to-light ratios and angular momenta of early-type fast-rotators and it allows for the inclusion of dark matter, supermassive central black holes, spatially varying anisotropy, and multiple kinematic components.

#### 4.6 Dispersion velocities versus rotation curves

Here, it is worth making a comparison between the circular velocity  $V(r)$  and the radial (or line-of-sight) velocity dispersion of an irrotational gravitational tracer with distribution  $\nu_*(r)$  and with anisotropy  $\beta(r)$ . From Eq. (16) we get:

$$(-\gamma_*(r) + 2(\beta(r) + \alpha(r))) \sigma_r^2(r) = V^2(r) \quad (19)$$

$\alpha(r)$  and  $\gamma_*(r)$  are the logarithmic derivatives of  $\sigma_{\text{l.o.s.}}$  and  $\nu_*$ . Let us notice that, in dispersion velocity supported systems, even in the case of isotropic orbits:  $\beta(r) = 0$ , it is necessary to know the spatial distribution of the tracers in order to make any inference on the DM distribution. Flat RC and flat dispersion velocity profiles do not necessarily indicate the same gravitational field.

#### 4.7 Masses in spheroids within half-light radii

We can measure the *total* mass enclosed within the half-light radius  $R_{1/2}$  by measuring  $\sigma_{\text{l.o.s.}}(R_{1/2})$  the line of sight velocity dispersion at this radius (Wolf et al. 2010). Since  $\sigma_{\text{tot}}^2 = \sigma_r^2 + \sigma_\theta^2 + \sigma_\phi^2 = (3 - 2\beta)\sigma_r^2$  we can write the Jeans equation as  $G M(r)r^{-1} = \sigma_{\text{tot}}^2(r) + \sigma_r^2(r)(-\gamma_* + \alpha - 3)$ . Let us define  $R_3$  as  $\gamma_*(R_3) = 3^4$  since  $\alpha(R_3) \ll 3$  from the observed  $\sigma_{\text{los}}(r)$  profiles, then, at  $R = R_3$ , we have, independently of the value of the anisotropy:

$$M(R_{1/2}) \approx 3G^{-1}\sigma_{\text{l.o.s.}}^2(R_{1/2})R_{1/2} \quad (20)$$

---

<sup>4</sup>  $R_3 \simeq 1.1 R_{1/2}$

APOSTLE cosmological hydro dynamical simulations have tested the validity and accuracy of this mass estimator and found that the resulting measurements are, at most, biased by 20% (Campbell et al. 2017).

#### 4.8 Tracer mass estimator

Given a number of  $N$  of tracers in dynamical pressure supported equilibrium with no systematic rotation and moving with l.o.s. velocities within a dark halo of mass profile  $M(r)$ , the TME is expressed as

$$M(r_{\text{out}}) = \frac{C}{GN} \sum_{i=1}^N V_{\text{l.o.s.,i}}^2 R_i^\epsilon. \quad (21)$$

The prefactor  $C$  depends on i) the slope  $\epsilon$  of the gravitational potential, assumed to be:  $\Phi(r) \propto \frac{v_0^2}{\epsilon} \left(\frac{a}{r}\right)^\epsilon$ ;  $v_0^2 \log\left(\frac{a}{r}\right)$  ( $\epsilon = 0$ ). ii) the ‘‘slope’’  $\gamma_*$  of the de-projected density profile of the tracers ( $\rho_{\text{trac}}(r) \propto r^{-\gamma_*}$ ) iii) the orbital anisotropy  $\beta$  of the tracers.

We then have  $C = \frac{(\epsilon + \gamma_* - 2\beta)}{I_{\epsilon,\beta}} r_{\text{out}}^{1-\epsilon}$  with  $r_{\text{out}}$  the distance of the outermost tracer and  $I_{\epsilon,\beta} = \frac{\pi^{1/2} \Gamma(\epsilon/2 + 1)}{4\Gamma((\epsilon/2 + 5)/2)} [\epsilon + 3 - \beta(\epsilon + 2)]$ , where  $\Gamma$  is the Gamma function (Watkins et al. 2010; An and Evans 2011).

The mass estimator in Eq. (21) performs very well, especially in the case in which the tracers are in random orbits, so that  $\beta = 0$  and for ellipticals where we have  $\alpha = 0 \pm 0.1$ . In these cases, the uncertainties on the two latter quantities do not bias the mass estimate.

#### 4.9 Weak lensing

We briefly recall here that weak gravitational lensing is a powerful tool for probing the dark matter distribution in galaxies (Schneider 1996; Hoekstra and Jain 2008; Munshi et al. 2008; Bartelmann and Maturi 2016). It is known that observed images of distant galaxies are coherently deformed by weak lensing effects caused by foreground matter distributions. These distortions enable the measurement of the mean mass profiles of foreground lensing galaxy through the stacking of the background shear fields (Zu and Mandelbaum 2015). To determine halo mass, we measure the excess surface mass density  $\Delta\Sigma(R) = \overline{\Sigma(< R)} - \Sigma(R)$ , which is the difference between the projected average surface mass within a circle of radius  $R$  and the surface density at that radius. The tangential shear  $\gamma_t$  is directly related to the above quantities through  $\Delta\Sigma(R) = \Sigma_{\text{crit}} \langle \gamma_t(R) \rangle$ , where  $\Sigma_c$  is the critical surface density defining the Einstein radius of the lens

$$\Sigma_c = \frac{c^2}{4\pi G} \frac{D_s}{D_l D_{ls}}, \quad (22)$$

where  $D_s$ ,  $D_l$ , and  $D_{ls}$  are the distances to the source, to the lens and the lens-source one, respectively. The lens equation relates  $\gamma_t$  with the distribution of matter in the lensing galaxy:

$$\gamma_t(R) = (\bar{\Sigma}(R) - \Sigma(R))/\Sigma_c, \quad (23)$$

where  $\Sigma(R) = 2 \int_0^\infty \rho(R, z) dz$  is the projected mass density of the object distorting the galaxy image, at projected radius  $R$  and  $\bar{\Sigma}(R) = \frac{2}{R^2} \int_0^R x \Sigma(x) dx$  is the mean projected mass density interior to the radius  $R$ .

#### 4.10 Strong lensing

Gravitational lensing occurring in very aligned galaxy-galaxy-observer structures magnifies and distorts the images of a distant galaxy providing us with relevant information on the mass structure of the intervening galaxy so as of the background source (see Treu 2010).

The lens system is axially symmetric, the radial coordinate  $r$  is related to cylindrical polar coordinates by  $r = \sqrt{\xi^2 + z^2}$  where  $\xi$  is the impact parameter measured from the center of the lens. The mean surface density inside the radius  $\xi$  is

$$\bar{\Sigma}(\xi) = \frac{1}{\pi \xi^2} \int_0^\xi 2\pi \xi' \Sigma(\xi') d\xi'. \quad (24)$$

The presence of an Einstein ring of radius  $R_E$ , at projected galactocentric distance  $\xi$  (see Fig. 6), allows us to obtain the projected total mass inside  $\xi$ :

$$(M_{\text{halo}}(\xi) + M_{\text{stars}}(\xi)) = \pi R_E^2 \Sigma_c. \quad (25)$$

#### 4.11 X-ray emission & hydrostatic equilibrium

Isolated ellipticals have an X-ray emitting halo of regular morphology, that, extends out to very large radii. The gravitating mass inside a radius  $r$ ,  $M(r)$  can be derived from their X-ray flux if the emitting gas is in hydrostatic equilibrium. From its density and the temperature profiles we obtain the total mass profile (Fabricant et al. 1984; Ettori and Fabian 2006:

$$M(< r) = \frac{kT_g(r)r}{G\mu m_p} \left( \frac{d \log \rho_g(r)}{d \log r} + \frac{d \log T_g(r)}{d \log r} \right), \quad (26)$$

where  $T_g$  is the (measured) ionised gas temperature,  $\rho_g$  the gas density,  $k$  is the Boltzmann's constant,  $\mu = 0.62$  is the mean molecular weight and  $m_p$  is the mass of the proton.

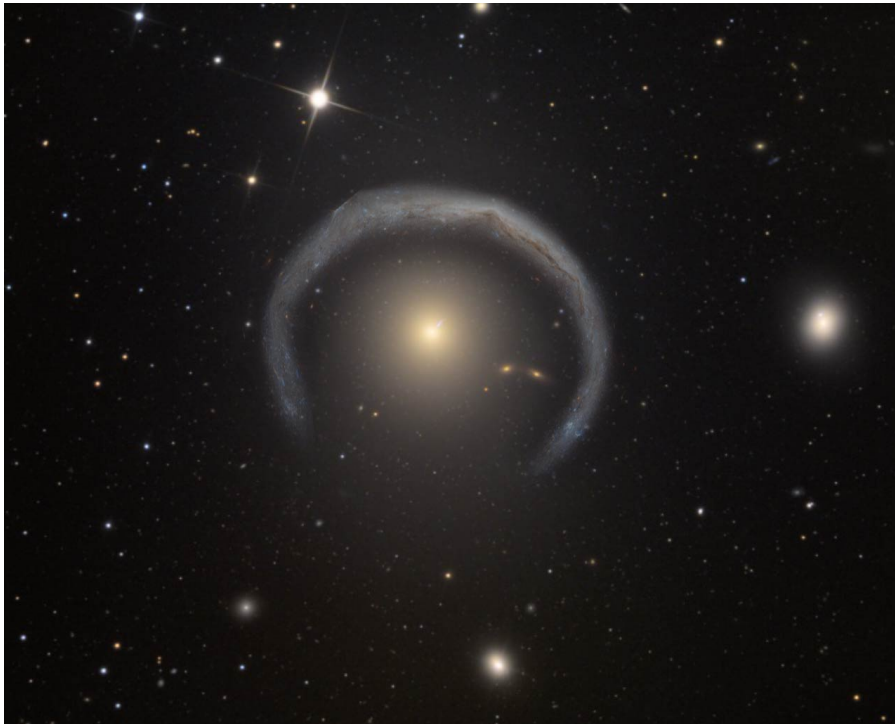


**Fig. 6** Einstein ring (artist's concept). This extraordinary GR effect provides us with the value of the projected mass of the galaxy lens inside  $R_E$ .

## 5 The mass of the stellar component in galaxies

We can assume that the stellar mass surface density  $\Sigma_*(r)$  is proportional to the luminosity surface density, which in galaxies is well measured by CCD infrared photometry. Radial variations of the  $M_*/L$  ratio exist and often are astrophysically relevant, but rarely they play a role in the determination of the mass profile of galaxies.

The total galaxy luminosity is related to its stellar content, hence, the direct approach to derive the galactic mass in stars by modelling their spectral energy distribution in terms of age, metallicity, initial mass function of the stellar component. This modelling, pioneered by Tinsley (1981), is performed by the well-known stellar population synthesis technique. The SED of a galaxy, selected colour indices and absorption lines are all reproduced by a theoretical models calculated under different assumptions regarding the above physical quantities. In practice, the exercise is not straightforward because degeneracies among age, metallicities, IMF and dust content, to name some, do arise and different combinations of the former quantities yield to very similar SEDs.

Bell and de Jong (2001) found rather simple relationships between mass-to-light ratios and certain colour indices. In detail, they investigated a suite

of spectrophotometric spiral galaxy evolution models that assumed a Salpeter Initial Mass Function, an exponentially declining star formation rate and a current age of 12 Gyr and found that the stellar mass to light ratios correlate tightly with galaxy colours (see also Bell et al. 2003).

The important stellar mass-to-light ratios in the Spitzer 3.6  $\mu\text{m}$  band ( $\Upsilon_{\star}^{3.6 \mu\text{m}}$ ) and in the K-band ( $\Upsilon_{\star}^K$ ) have also been derived by constructing stellar population synthesis models, with various sets of metallicity and star-formation histories (see Oh et al. 2008; de Blok et al. 2008).

We have

$$\log(\Upsilon_{\star}^K) = 1.43 \times (J - K) - 1.38 \quad \Upsilon_{\star}^{3.6 \mu\text{m}} = 0.92 \Upsilon_{\star}^K - 0.05. \quad (27)$$

The values of the galaxy stellar masses as derived from their SEDs have been compared with those obtained by other methods. Grillo et al. (2009) investigated a sample of ellipticals with Einstein rings from which they derived the total projected mass (dominated by the stellar component) and, from the latter, the total mass of the spheroid. Then, by using the SDSS multicolour photometry they fitted the galaxy spectral energy distributions (SEDs) by means of composite stellar-population synthesis models of Bruzual and Charlot (2003) and Maraston (2013) and obtained the photometric mass of the stellar spheroid. The two different mass estimates agreed within 0.2 dex (see also Tirit et al. (2011)).

Salucci et al. (2008) have estimated kinematically the disk mass from the rotation curve of 18 spirals of different luminosity and Hubble types and have compared them with the values obtained by fitting their SED with spectrophotometric models. They found  $M_{\text{pho}} \propto M_{\text{kin}}^{1.0 \pm 0.1}$  with a r.m.s. of 40% suggesting that photometric and kinematical estimate of the masses of the stellar galaxy disks are statistically consistent.

We have to caution about one consequence of the found disagreement of about 0.15 dex among the dynamical and the spectro-photometric estimates. This value is small to affect existing color stellar mass relationships, but it is large if we want to use it for mass modelling purposes. In fact, in spirals, for  $R < R_D$ , the dark and the luminous components of the circular velocity are of the same order of magnitude  $V_h \simeq V_d (M_{D,\text{true}}/M_{D,\text{phot}})^{-0.5}$  and therefore an uncertainty of  $(10^{0.15} - 1) 100\% \sim 40\%$  on the value of  $M_{D,\text{phot}}$  jeopardizes the derivation of the DM velocity contribution and even more that of the subsequent DM halo density.

For spiral galaxies there is a reliable method to estimate the disk mass which is immune from the latter uncertainty. We start from the gravitating mass inside  $R_{\text{opt}}$ :  $M_g(R_{\text{opt}}) \equiv G^{-1} V_{\text{opt}}^2 R_{\text{opt}}$  and  $\nabla$ , the rotation curve logarithmic slope measured at  $R_{\text{opt}}$ :  $\nabla \simeq 3.2(1 - V(2.2 R_D)/V(R_{\text{opt}}))$ . From Persic and Salucci (1990) we have:

$$M_D = (0.72 - 0.85\nabla) M_g(R_{\text{opt}}), \quad (28)$$

where the disk mass has uncertainty of 20%.

## 6 DM halo profiles

In this section, we will introduce the DM halo profiles that are presently adopted: the empirical ones and those emerging from specific theoretical scenarios, see Fig. 7. It is useful to remind that  $M_h(r) = G^{-1}V_h^2(r)r = \int_0^r 4\pi r'^2 \rho_h(r') dr'$  with  $V_h(r)$  the halo contribution to the circular velocity  $V(R)$ .

### BT-URC

The empirical DM halo density profile, adopted for the URC of Persic, Salucci and Stel (1996), takes the form (see also Binney and Tremaine 2008)

$$\rho_{\text{BT-URC}}(r) = \frac{1}{G} \frac{v_0^2(r^2 + 3r_0^2)}{(r_0^2 + r^2)^2}, \quad M_{\text{BT-URC}}(r) = \frac{1}{G} \frac{v_0^2 r^3}{r_0^2 + r^2}, \quad (29)$$

where  $r_0$  and  $v_0$  are the core radius and the asymptotic circular velocity of the halo, respectively.

### Navarro–Frenk–White

In  $\Lambda$ CDM the structure of virialized DM halos, obtained by  $N$ -body simulations, have a universal spherically averaged density profile,  $\rho_{\text{NFW}}(r)$  (Navarro et al. 1997):

$$\rho_{\text{NFW}}(r) = \frac{\rho_s}{(r/r_s)(1 + r/r_s)^2}, \quad (30)$$

where  $\rho_s$  and  $r_s$  are strongly correlated:  $r_s \simeq 8.8 \left( \frac{M_{\text{vir}}}{10^{11} M_\odot} \right)^{0.46}$  kpc (e.g., Wechsler et al. 2006). We define  $X \equiv r/R_{\text{vir}}$ , the concentration parameter  $c \equiv r_s/R_{\text{vir}}$  is a weak function of mass (Klypin et al. 2010):

$$c = 9.35 \left( \frac{M_{\text{vir}}}{10^{12} M_\odot} \right)^{-0.13} \quad (31)$$

but a very important quantity in determining the density shape at intermediate radii. The circular velocity for an NFW dark matter halo is given by

$$V_{\text{NFW}}(X) = V_{\text{vir}}^2 \frac{1}{X} \frac{\ln(1 + cX) - \frac{cX}{1+cX}}{\ln(1+c) - \frac{c}{1+c}}, \quad (32)$$

with  $M_{\text{vir}} = 100 \frac{4}{3}\pi \rho_c R_{\text{vir}}^3$  and  $\rho_c = 1.0 \times 10^{-29}$  g/cm<sup>3</sup>.

### Burkert-URC

The Burkert empirical profile (Burkert 1995; Salucci and Burkert 2000) well reproduces, in cooperation with the velocity components of the stellar and gaseous disks, the individual circular velocities of spirals, dwarf disks and low surface brightness systems. Furthermore, this profile is at the basis of the universal rotation curve of the above systems. The density profile reads as

$$\rho_{\text{B-URC}}(r) = \frac{\rho_0 r_0^3}{(r + r_0)(r^2 + r_0^2)}, \quad (33)$$

$r_0$  and  $\rho_0$  are the core radius and central density respectively. The velocity profile is:

$$V_{\text{B-URC}}^2(r) = \frac{G}{r} 2\pi\rho_0 r_0^3 [\ln(1 + r/r_0)] + \frac{1}{2} \ln(1 + r^2/r_0^2) - \tan^{-1}(r/r_0). \quad (34)$$

This profile represents the (empirical) family of cored distributions (see Fig. 7). To discriminate among them the correct one is, currently, very difficult. It would require a large number of accurate measurements of RCs at inner radii  $r < r_0$ .

### Pseudo-isothermal profile

The PI halo profile  $\rho_{\text{PI}}(r) = \frac{\rho_0 r_0^2}{(r^2 + r_0^2)}$  is an alternative cored distribution to Eq. (34). This density profile implies that  $V_{\text{PI}}(r) = \text{const}$  for  $r \gg R_{\text{opt}}$ , which disagrees with the RC profiles at very outer radii that show a decline with radius (Salucci et al. 2007).

### Fermionic halos

In this scenario there is a strong degeneracy limit for which the DM particles velocity dispersion  $\sigma_{\text{DM,min}}^2(\rho)$  has the minimal value. This represents the most compact configuration for a self-gravitating fermionic halo (see e.g., Di Paolo et al. 2018). The density profiles of such fully degenerate halos are universal, depending only on the mass of the configuration:

$$\rho(x) = \rho_0 \cos^3 \left[ \frac{25}{88} \pi x \right], \quad x = r/R_h, \quad (35)$$

where  $\rho_0$  is the central DM halo density. This profile is quite peculiar and recognizable in the RCs.



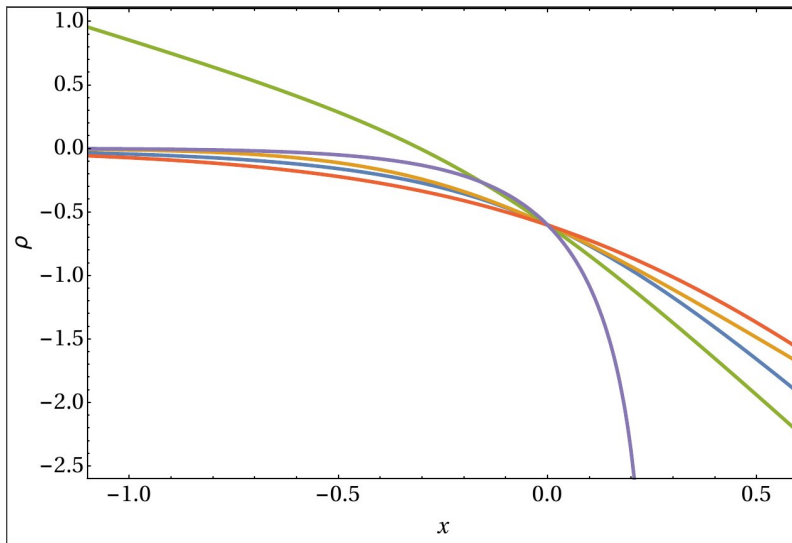


**Fig. 7** DM halos density profiles. NFW (*green*), Burkert-URC (*blue*), fully degenerate fermionic particles (*violet*), Pseudo Isothermal (*yellow*) and Binney-URC (*red*).

### Zhao halos

The following density profile (Zhao 1996):

$$\rho(r) = \frac{\rho_0}{\left(\frac{r}{R_0}\right)^\gamma \left(1 + \left(\frac{r}{R_0}\right)^\alpha\right)^{\frac{\beta+\gamma}{\alpha}}}, \quad (36)$$

where  $\rho_0$  is the central density and  $R_0$  the “core radius”, that, initially, was not proposed for the DM halo density, is defined by the set of parameters:  $\alpha$ ,  $\beta$ ,  $\gamma$ . The case  $(1, 3, \gamma)$  is sometimes used as a “cored-NFW” profile. This is incorrect because both in the Burkert and in the NFW profiles, the inner regions are not related with the outermost regions, as, instead occurs in the Zhao model. Moreover, with the latter, we pass from the two free parameters of most of the halo models in the ballpark, to the five of Eq. (36). This seems in disagreement with observations in spirals, ellipticals and spheroidals that suggest that DM halos are one (two)-parameters family.

### Transformed halos

We want to draw the attention on the profiles which are the outcome of the primordial NFW halos after that these have experienced the effects that it is called baryonic feedback (e.g., Di Cintio et al. 2014). They seem in agreement with those observed around galaxies. However, the collisionless DM paradigm requires that such kind of transformation has occurred in every galaxy of any luminosity and Hubble type and to reach this goal seems extremely difficult.

On the other side, the effect of the baryonic feedback to DM halos has to be investigated, no matter what the nature of DM is. In conclusion, a review on this crucial complex and still on its infancy issue must be a goal future work.

## 7 Kinematics of galaxy systems

A main channel to obtain the DM properties in galaxies is through their kinematics (rotation curves and dispersion velocities). The analysis could regard individual objects or stacked data of a sample of objects.

### 7.1 The Tully–Fisher and the Baryonic Tully–Fisher

Tully and Fisher (1977) discovered that, in spirals, the neutral hydrogen 21-cm FWHM linewidths  $w_{50}$ , related, in a disk system, to the maximal rotational velocities  $V_{\max}$  by:  $\log V_{\max} \simeq -0.3 + \log w_{50} - \log \sin i$ , with  $i$  the inclination of the galaxy with respect to the l.o.s., correlate with the galaxy magnitudes  $M$

$$M = a \log \left( \frac{w_{50}}{\sin i} \right) + b, \quad (37)$$

where  $a$  is the slope of the relationship and  $b$  the zero-point.

With the availability of a large number of extended RCs, the relation evolved: a radius proportional to the disk length-scale  $R_D$  (e.g.  $R_{\text{opt}}$  or  $R_{\max} = 2.2 R_D$ ) emerged as the reference radius; moreover, the circular velocity at this reference radius substituted the linewidth  $w$ .

It is easy to realize that Eq. 37 just reflects the equilibrium configuration of rotating disks embedded in dark halos (Strauss and Willick 1995) and that the magnitude  $M$  in the relation is the prior for the stellar disk mass. However, it is worth going deeper: in fact, despite that in each spiral the disk and the dark components contribute in different proportions to the value of  $V(R_{\text{opt}}) = (V_d(R_{\text{opt}})^2 + V_h(R_{\text{opt}})^2)^{1/2}$ , one finds that  $V_d(R_{\text{opt}})$  correlates better with magnitudes than  $V(R_{\text{opt}})$  (Salucci et al. 1993). This finding can be understood in that the latter relationship couples two attributes that pertain exclusively to the stellar disk: its mass, measured kinematically and its luminosity.

The physical meaning of the TF relation as a link between circular velocities and stellar masses has been shown by means of 729 kinematically and morphologically different galaxies belonging to the SAMI Galaxy Survey sample (Bloom et al. 2017). It has been found:

$$\log V_{2.2} = (0.26 \pm 0.017) \log(M_*/M_\odot) - (0.5 \pm 0.13), \quad (38)$$

with  $V_{2.2} \equiv V(2.2R_D)$ . Such relationship results in very good agreement with the correspondent one we can derive from the URC (Salucci et al. 2007):  $\log V_{2.2} = (0.263 \pm 0.005) \log(M_*/M_\odot) - (0.57 \pm 0.05)$ .

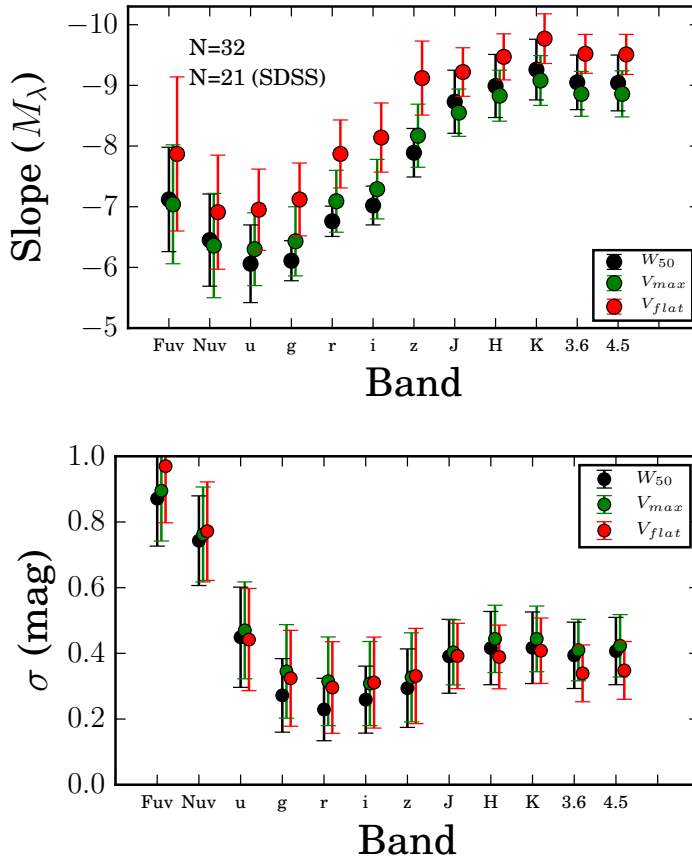


**Fig. 8** The slope and the scatter of the TF relation by adopting different reference velocities and different systems of magnitude.

A recent work (Ponomareva et al. 2018) has investigated the statistical properties of the Tully–Fisher relation for a sample of 32 galaxies with accurately measured distances and with 1) panchromatic photometry in 12 bands: from far ultra-violet to  $4.5 \mu\text{m}$ , and 2) spatially resolved HI kinematics. For this sample they adopted, in turn, the following reference velocities: the linewidth  $W_{50}$ , the maximum velocity  $V_{max}$  and  $V_{flat}$  the average value of the RC in the range  $(2-5) R_D$ . With these quantities they constructed 36 correlations, each of them involving one magnitude and one kinematical parameter. They found that the slope of the relationships strongly depends on the band considered and that the tightest correlation occurs between the  $3.6 \mu\text{m}$  photometric band magnitude  $M_{3.6 \mu\text{m}}$  and  $V_{flat}$  (see Fig. 8):

$$M_{3.6} = (9.5 \pm 0.3) \log V_{flat} + (3.3 \pm 1.7) \quad (39)$$

in good agreement with the value of  $8.6 \pm 0.1$  found by Yegorova and Salucci (2007) for the slope of the I magnitude of the radial Tully–Fisher relationship at  $R = 1.2 R_{\text{opt}}$  that becomes  $9.6 \pm 0.3$  when translated in the  $3.6 \mu\text{m}$  band.

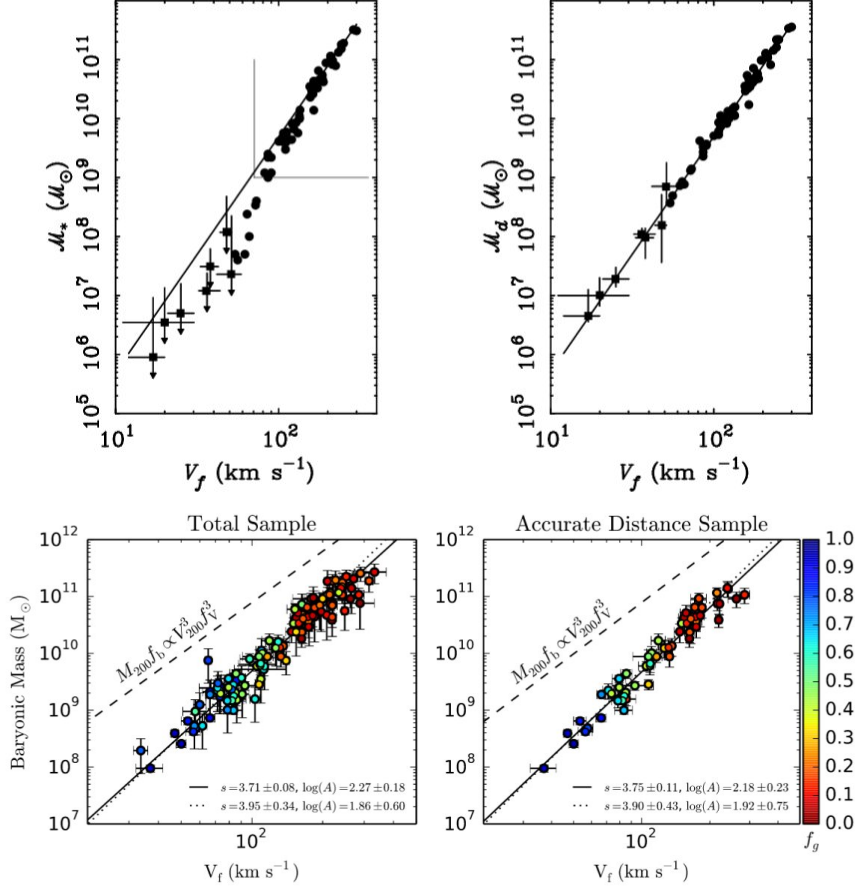


**Fig. 9** (top) The stellar mass (*left*) and baryonic (*right*) Tully–Fisher relations. (bottom) The determination of the BTF. Images reproduced with permission from [top] McGaugh (2005), and [bottom] from Lelli et al. (2016a), copyright by AAS.

## 7.2 The Baryonic Tully–Fisher

McGaugh et al. (2000) found a fundamental relationship by correlating the baryonic mass (i.e., the sum of the stellar and the (HI + He) gas mass) with the reference rotation velocity  $V_{\text{flat}}$ . This Baryonic Tully–Fisher (BTF) relation has been thorough fully studied and confirmed by several works: (e.g., Bell and

de Jong 2001; Verheijen 2001; Gurovich et al. 2004). A decisive step forward in understanding it came from McGaugh (2005), who investigated a sample of galaxies with extended 21-cm rotation curves spanning the range  $20 \text{ km s}^{-1} < V_{\text{flat}} < 300 \text{ km s}^{-1}$ . By using a grid of stellar population models they estimated the values of the stellar disks masses to which they added those of the HI disks derived by the observed 21-cm HI fluxes. They found:

$$M_{\text{bar}} = A V_{\text{flat}}^4; \quad A = 50 M_{\odot} \text{ km}^{-4} \text{ s}^{-4} \quad (40)$$

(see Fig. 9). Notice that, by including the HI mass in the galaxy baryonic mass, the BTF becomes log-log linear and has less intrinsic scatter.

Lelli et al. (2016a) investigated the BTF relationship with a sample of 118 disc galaxies (spirals and irregulars) with data of the highest quality: extended HI high quality rotation curves tracing the total mass distribution and Spitzer photometry at  $3.6 \mu\text{m}$  tracing the stellar mass distribution. They assumed the stellar mass-to-light ratio ( $M_{\star}/L_{3.6 \mu\text{m}}$ ) to be constant among spirals and found that the scatter, slope, and normalization of the relation vary with the adopted  $M_{\star}/L_{3.6 \mu\text{m}}$  value, though the intrinsic scatter is always modest:  $\leq 0.1$  dex. The BTF relationship gets minimized for  $M_{\star}/L_{3.6 \mu\text{m}} > 0.5$ . This result, in conjunction with the RC profiles of the galaxies in the sample, implies maximal discs in the high-surface-brightness.<sup>5</sup>

The BTF relationship slope comes close to 4.0, see Fig. 9(bottom) and the residuals show no correlation with the galaxy structural parameters (radius or surface brightness). The above relationship seems to play an important cosmological role, however, the value of its slope strongly depends on the vagueness in the definition of the reference velocity  $V_{\text{flat}}$  (Brook et al. 2016). The DM enters in this relation principally through the value of the dark/ total matter fraction at  $R_{\text{flat}}$ : this indicates that the BTF is related more to the disk formation process than to the DM nature.

### 7.3 The universal rotation curve and the radial Tully–Fisher

We can represent all the rotation curves of spirals by means of the universal rotation curve (URC), pioneered in Rubin et al. (1980), expressed in Persic and Salucci (1991) and set in Persic, Salucci and Stel (1996) and in Salucci et al. (2007). By adopting the normalized radial coordinate  $x \equiv r/R_{\text{opt}}$ , the RCs of spirals are very well described by a universal profile, function of  $x$  and of  $\lambda$ , where  $\lambda$  is one, at choice, among  $M_I$ , the I magnitude,  $M_D$ , the disk mass and  $M_{\text{vir}}$ , the halo virial mass (Salucci et al. 2007).

The universal magnitude-dependent profile is evident in the 11 *coadded* rotation curves  $V_{\text{coadd}}(x, M_I)$  (Fig. 6 of Persic, Salucci and Stel 1996 and top of Fig. 11), built from the individual RCs of a sample of 967 spirals with luminosities spanning their whole I-band range:  $-16.3 < M_I < -23.4$ . I-band

<sup>5</sup> Notice that maximal discs are incompatible with cuspy DM halos (van Albada et al. 1985).

surface photometry measurements provided these objects with their stellar disk length scales  $R_D$  (Persic and Salucci 1995).<sup>6</sup>

The coadded RCs are built in a three-step way: **1)** We start with a large sample of galaxies with RC and suitable photometry (in the case of Persic, Salucci and Stel (1996): 967 objects and suitable I-band measurements). The whole (I) magnitude range is divided in 11 successive bins centred at  $M_I$ , as listed in Table 1 of Persic, Salucci and Stel (1996). **2)** The RC of each galaxy of the sample is assigned to its corresponding I magnitude bin, normalized by its  $V(R_{\text{opt}})$  value and then expressed in terms of its normalized radial coordinate  $x$ . **3)** The double-normalized RCs  $V(x)/V_{\text{opt}}$  curves are coadded in 11 magnitude bins and in 20 radial bins of length 0.1 and then averaged to get:  $V_{\text{coadd}}(x, M_I)/V_{\text{coadd}}(1, M_I)$ , the points with errorbars in Fig. 11. The 11 values of  $V_{\text{coadd}}(1, M_I)$  are given in Table 1 of Persic, Salucci and Stel (1996). The RCs are usually increasing or decreasing. Simplifying, they increase when they are dark matter dominated or always for  $r < R_D$  and decrease for  $r > 2R_D$  when they are disk dominated.<sup>7</sup> The recent finding of RCs of six massive star-forming galaxies that, outside  $R_{\text{opt}}$ , decrease with radius (Genzel et al. 2017) has been considered very surprising. Rightly, it has been proposed that this trend arises because this high-redshift galaxy population was strongly baryon dominated. However, while the importance of such objects in the cosmological context is obvious, there is a presence, also in the local Universe, of many baryon dominated decreasing RCs. This was first drawn to the attention by Persic and Salucci (1991) and, moreover, it is inbuilt in the URC.

The URC is the analytical function devised to fit the stacked/coadded RCs  $V_{\text{coadd}}(x, M_I)$ . In principle, it could be any suitable empirical function of  $(x, M_I)$ , the idea of Persic, Salucci and Stel (1996) was to choose, as fitting function, the sum in quadrature of the velocity components to the circular velocity. Namely, the Freeman stellar disk with one free parameter, its mass  $M_D$  and the dark halo with an assumed profile and two free parameters, the central density  $\rho_0$  and the core radius  $r_0$ . Then, the data  $V_{\text{coadd}}(x, M_I)$  are fitted by the  $V_{\text{URC}}$  universal function:

$$V_{\text{URC}}^2(x, M_I) \equiv V_{\text{URCd}}^2(x; M_D(M_I)) + V_{\text{URCh}}^2(x; \rho_0(M_I), r_0(M_I)) \quad (41)$$

The first component of the RHS is the standard Freeman disk of Eq. (8), the second is the B-URC halo of Eq. (34). In dwarf galaxies, a HI term must be included (Karukes and Salucci 2017).

The excellent fit (see Fig. 11) has led us to the validation of the URC idea: there exists a universal function of (normalized) radius and luminosity that well fits the RC of any spiral galaxy (see Salucci et al. 2007).<sup>8</sup>

<sup>6</sup> See also Lapi et al. (2018) for the analysis of 24 *coadded* RCs obtained from 3500 individual RCs.

<sup>7</sup> We stress that only the RCs with  $190 \text{ km/s} < V_{\text{opt}} < 230 \text{ km/s}$  and in the radial range  $1 R_D < R < 4 R_D$  can be considered flattish.

<sup>8</sup> In short: the variance of  $V(x, L)$  is negligible, i.e., the r.m.s. of the values of the RCs in galaxies of same luminosity  $L$  and at the same radius  $x$  is negligible.

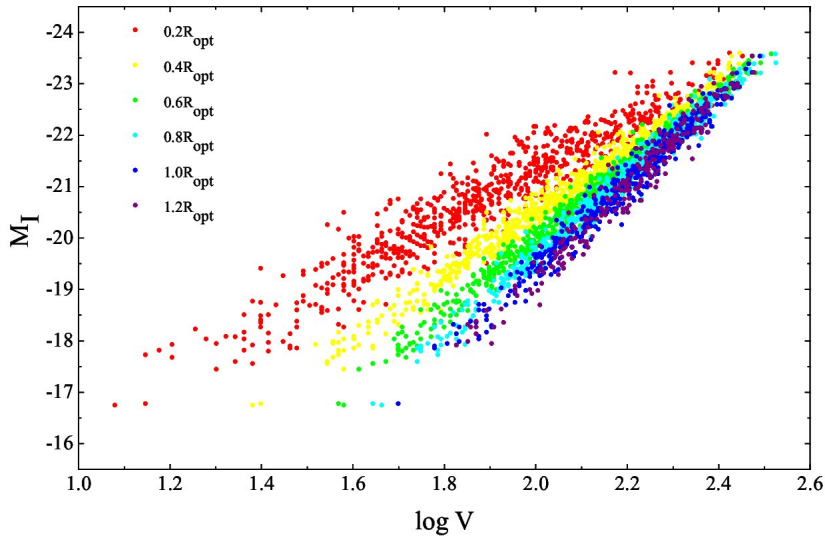


**Fig. 10** The radial TF. The variation of the slopes  $a_i$  with  $r_i$  is very evident. Image reproduced with permission from Yegorova and Salucci (2007), copyright by the authors.

The radial Tully–Fisher is a relationship *on* the URC surface, orthogonal to the various RCs (Yegorova and Salucci 2007; see Fig. 10 top). At different galactocentric distances, measured in units of the optical size,  $r_i \equiv i R_{\text{opt}}$  ( $i = 0.2, 0.3, \dots, 1$ ), a family of independent Tully–Fisher-like relationships emerges:

$$M_{\text{band}} = b_i + a_i \log V(r_i), \quad (42)$$

with  $M_{\text{band}}$  the magnitude in a specific band, often the (R, I)-bands. The RTF has a very small r.m.s. scatter, at any radius smaller than that of the classical TF. It also shows a large systematic variation of the slopes  $a_i$  with  $r_i$  that range, across the disk, between  $-4$  and  $-8$ . This variation, in cooperation with the smallness of the scatter, indicates that the fractional amount of dark matter inside the optical radius is luminosity-dependent (Yegorova and Salucci 2007).

It is important to stress that, given a sample of RCs, the RTF relationship provides us with an independent method of deriving (if it exists) the underlying coadded RCs and, in turn, the relative URC. Yegorova and Salucci (2007), in fact, have shown that samples with a similar  $a_i$  vs  $r_i$  relationship have also similar  $V_{\text{coadd}}(x, \text{magnitude})$ . This has been applied to the large samples of Courteau (1997) and Vogt et al. (2004a,b) with the result of finding the same RTF discovered in the Persic, Salucci and Stel (1996) sample (see Fig. 8 of Yegorova and Salucci 2007) and, then, finding very similar coadded RCs.

## 8 The dark matter distribution in disk systems

The general pattern is the following: spirals show a reference radius  $R_T(L_I)$  whose size ranges from 1 to  $3 R_D$  according to the galaxy luminosity (see Fig. 8 of Persic, Salucci and Stel (1996) and Palunas and Williams (2000)); inside  $R_T(L_I)$  the ordinary baryonic matter fully accounts for the RC, while, for  $R > R_T(L_I)$ , is instead unable to justify the profile and the amplitude of the RC.

### 8.1 Dark matter from stacked RCs

Very extended individual RCs and virial velocities  $V_{\text{vir}} \equiv (GM_{\text{vir}}/R_{\text{vir}})^{1/2}$  obtained in Shankar et al. (2006), further support the URC paradigm and help determining the universal velocity function out to the virial radius (Salucci et al. 2007). It is important to stress that the  $V_{\text{URC}}$  function (and the relative mass model) has, in principle, three free parameters: the disk mass and two quantities related to the DM distribution (the halo central density  $\rho_0$  and the core radius  $r_0$ ). These are obtained by best fitting the  $V_{\text{coadd}}(x, M_I)$  and found to be correlated among themselves and with the luminosity. So, the RCs and the related gravitational potential of spirals belong to a family ruled by 1-parameter that we can choose among many possibilities, e.g., the halo mass, which is a combination of  $\rho_0$  and  $r_0$  and it ranges in spirals as:  $3 \times 10^{10} M_{\odot} \leq M_{\text{vir}} \leq 3 \times 10^{13} M_{\odot}$ .

### 8.2 Dark matter from individual RCs

The study of individual RCs is very similar to that of the stacked ones as regard to their mass modelling, but it is complementary to it with respect to the data analysis. Moreover, in the core-cusp issue, the individual RCs have a special role: stacked RCs of spirals, as seen in the previous section, points unambiguously to a cored distribution, but cannot indicate to us whether this is a sort of average property of the entire population of spirals or a property of any single object. Only the analysis of fair number of individual RCs of systems of different luminosity and Hubble types can answer to this.

It is worth pointing out that, in the first 15 years since the DM discovery from the profiles of the RCs, the latter have always been reproduced by models including a Freeman disk, a bulge and a dark halo with the *cored* Pseudo Isothermal distribution (e.g., Carignan and Freeman 1985; van Albada et al. 1985). It is well-known that in the current  $\Lambda$ CDM cosmological scenario the dark matter halos have a very specific and universal cusped density distribution (Navarro et al. 1997). A debate has arisen on the level of the observational support for such profile (de Blok et al. 2001; Salucci 2001; Gentile et al. 2004; Simon 2005; Spekkens et al. 2005; Kuzio de Naray et al. 2008; de Blok et al.



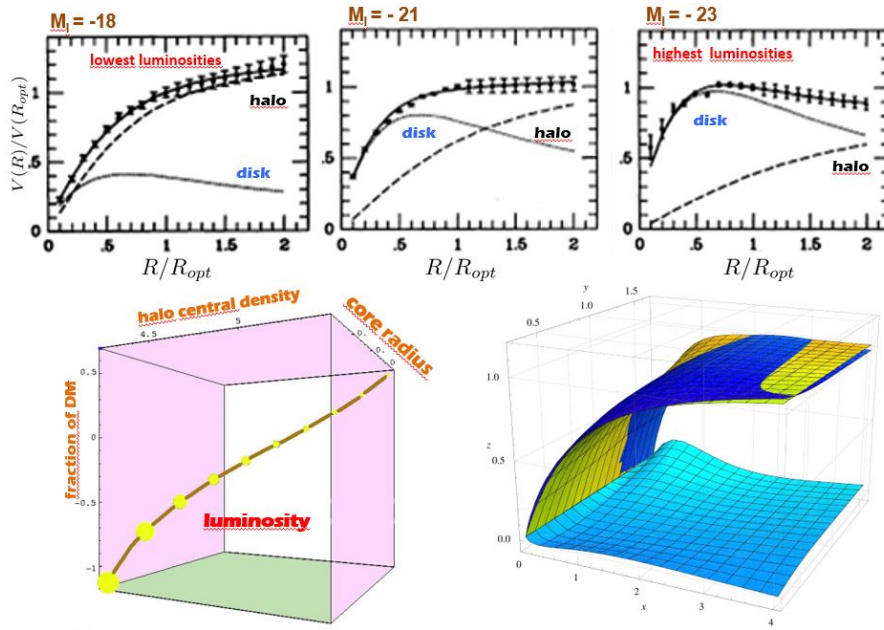


**Fig. 11 (top)** The URC best-fit models of the coadded RCs (*points with errorbars*) (Percic, Salucci and Stel 1996). It is shown: the bin magnitude  $M_I$ , the disk/halo contributions (*dotted/dashed lines*) and the resulting URC (*solid line*). **(bottom left)**. The 4-D relationship among the central DM density, its core radius in units of  $R_{opt}$ , the DM fraction at  $R_{opt}$  and the galaxy I-luminosity (proportional to the area of the circles). **(bottom right)**. The URCs from Percic, Salucci and Stel (1996), (*yellow*) and from Catinella et al. (2006) (*blue*). Legend:  $x \equiv R/R_D$ ,  $y \equiv \log(M_{vir}/(10^{11} M_\odot))$ ,  $z \equiv V(x)/V(3.2)$ . The differences between the two URCs are also indicated.

2008; Oh et al. 2011; Adams et al. 2014 to name a few, reviews on this issue: Bullock and Boylan-Kolchin 2017; de Blok 2010).<sup>9</sup>

It is important to remark that the DM cores could come *ab initio* from the structural properties of the (exotic?) DM particles or been created, over all the Hubble time, by dynamical processes occurring inside the galaxies.

Martinsson et al. (2013) devised and applied to a sample of 30 spirals, a method to decompose the rotation curves in its dark and luminous components. The method exploits the vertical velocity dispersions of the disk stars  $\sigma_z$  (see Sect. 6.3). By reminding that  $R_{max} \equiv 2.2 R_D$  is the radius where the disk velocity component has its maximum, they found:  $(V_d(R_{max})/V(R_{max}))^2 = 0.57 \pm 0.07$ , with a dependence on galaxy luminosity: in their velocity models, at  $R_{max}$ , the disk component prevails over the dark component in the biggest spirals, while, it is very sub-dominant in the smallest ones.

They also modeled the dark matter halos with either a PI or a NFW profile and found the former distribution performing something better and showing

<sup>9</sup> Let us stress that, in this issue, non circular motions in the RCs play a minor role (Oh et al. 2008; Gentile et al. 2005).

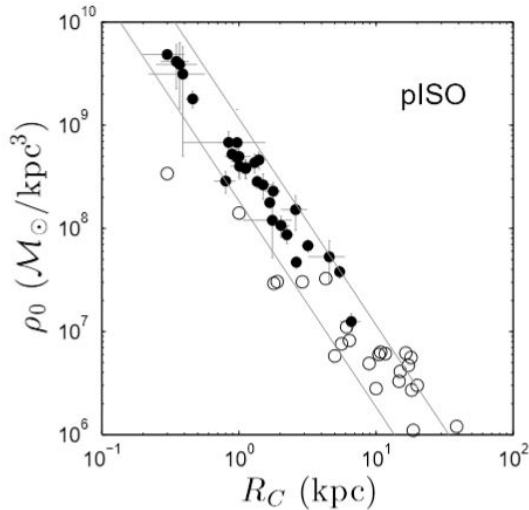


**Fig. 12** The relationship between the size of the DM core radius  $R_C$  and the value of the central dark matter density  $\rho_0$ . Image reproduced with permission from Martinsson et al. (2013), copyright by ESO.

a tight  $\rho_0$  vs.  $r_0$  relationship, very similar to that found in spirals by means of a different analysis (see Fig. 12).

A recent study of NGC5005 (Richards et al. 2015) can be considered as a test case investigation of the mass distribution in spirals obtained by means of multi-messenger observations. These included images taken at  $3.6 \mu\text{m}$  from the Spitzer Space Telescope, B and R broadband and  $\text{H}\alpha$  narrowband observations. Very Large Array (VLA) radio synthesis observations of neutral hydrogen provided the HI surface density and the kinematics. Spectroscopic integral field unit observations at WIYN 3.5-m telescope provided the ionized gas kinematics in the inner region. The surface brightness has been carefully decomposed in its disk and bulge component. The modelling of the composite high resolution rotation curve clearly favors a PI DM halo, with core radius of  $2.5 \pm 0.1$  kpc, over the corresponding NFW configuration.

Bottema and Pestaña (2015) obtained high resolution kinematics for sample of 12 galaxies, whose luminosities are distributed regularly over a range spanning several orders of magnitude. They found that models with maximum disks, cored DM halos and a unique value of the mass-to-light ratio, i.e.  $M_D/L_R = 1.0$ , fit very well all the RCs, see Fig. 13. NFW DM halos, independently of the baryonic distribution, cannot fit the RCs of the least massive galaxies of the sample, while, for the most massive ones, the best fitting values of the structural parameters of the NFW +stellar/HI disks models, namely the halo concentration and mass and the mass-to-light ratio of the stellar disk, take often non-physical values.

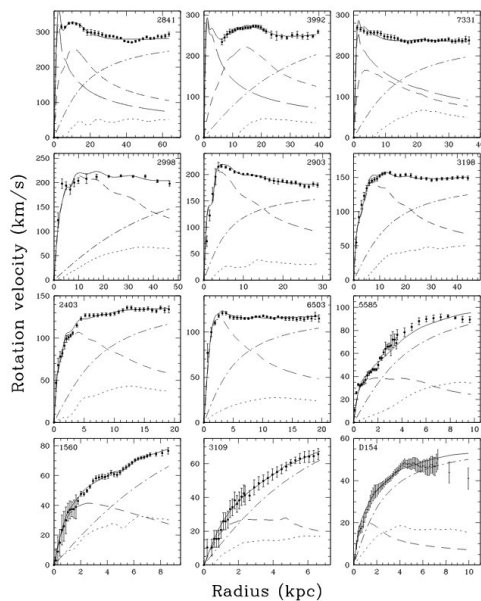


**Fig. 13** Maximum disc best-fits (*solid lines*) to the RCs (*dots with errorbars*). Also shown the contribution of gas, disc, bulge, and PI dark halo (*dotted, short dashed, long dashed, dash-dot lines*). Image reproduced with permission from Bottema and Pestaña (2015), copyright by the authors.

The Spitzer Photometry & Accurate Rotation Curves sample includes 175 nearby galaxies with surface photometry at  $3.6 \mu\text{m}$  and high-quality rotation curves. This sample spans a broad range of morphologies (S0 to Irr), luminosities ( $\sim 5$  dex), and surface brightness ( $\sim 4$  dex). These data have been used by Lelli et al. (2016b) in order to build the mass models of the galaxies. They adopted the specific value of 0.5 for the stellar mass-to light ratio in the  $3.6 \mu\text{m}$ -band as suggested by stellar population models and found that  $V_{\text{bary}}/V$  varies with luminosity and surface brightness: the stellar disks in high-mass, high-surface-brightness galaxies are nearly maximal, while in low-mass, low-surface-brightness galaxies they are very submaximal. Moreover, in these galaxies, the cored DM halo + (high mass) stellar disk model, generally, reproduces the sample RCs very well, differently from the cuspy halo + (low-mass) stellar disk model that often shows a bad fit and/or non-physical values for the parameters of the mass model.

The mass distribution of 121 nearby objects with high quality optical rotation curves has been recently derived from the Fabry–Pérot kinematical GHASP survey of spirals and irregular galaxies (Korsaga et al. 2018). These galaxies cover all morphological types of spirals and have infra-red  $3.6 \mu\text{m}$  emission measurements, good tracers the old stellar population. Combining the kinematical and the surface brightness data they obtained the mass models once they assumed a specific DM halo density profile. They considered the

PI cored profile and the Navarro–Frenk–White cuspy profile. The value of the  $M_D/L_{3.6}$  for the stellar disc was obtained for each objects in two different ways: 1) from the stellar evolutionary models and the WISE  $W_1$ - $W_2$  colours, 2) from fitting the RC. Both approaches found that: (i) the rotation curves of most galaxies are better fitted with a cored rather than with a cuspy profile, (ii) there are luminosity/Hubble type dependent relationships between the parameters of the DM and those of the luminous matter. In detail, in the PI halos framework they found that core radius  $\propto$  (central DM halo density) $^{-1}$ , in very good agreement with Kormendy and Freeman (2004); Donato et al. (2009). In the NFW framework they found a very strong dependence of the concentration on the halo virial mass, in disagreement with the outcome of N-body simulations (e.g., Klypin et al. 2010).

### 8.2.1 The Galaxy

The investigation of DM distribution in our Galaxy is clearly important under many aspects, although it is made difficult by our location inside it. The stellar component can be modeled as a Freeman exponential thin disk of length scale  $R_D = (2.5 \pm 0.2)$  kpc (e.g., Juric et al. 2008).

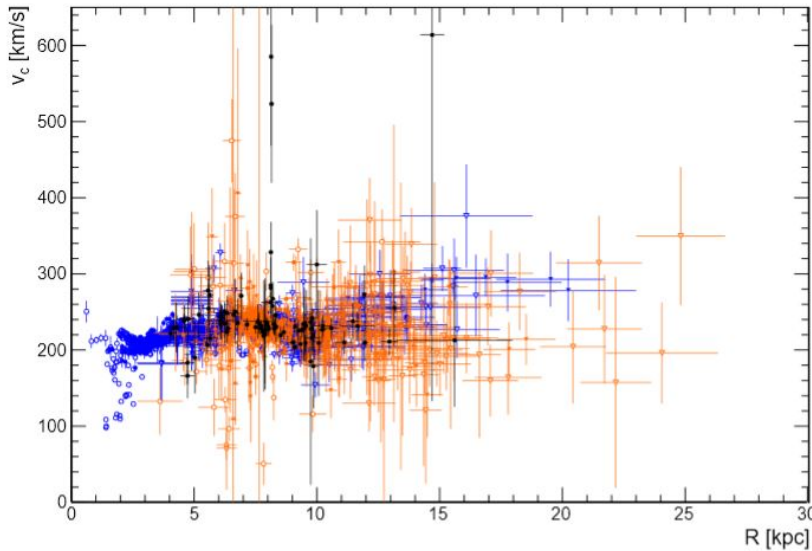


**Fig. 14** Rotational velocities in the Milky Way derived from gas and stellar kinematics (*blue, orange*) and masers measurements (*black*). Notice measurements with huge uncertainty. Image reproduced with permission from Pato and Iocco (2017), copyright by the authors.

Very precise measurements of position and proper motion of maser sources (Honma et al. 2012) provide us with a reliable solar galactocentric distance of

$R_\odot = 8.29 \pm 0.16$  kpc and a circular speed, at  $R_\odot$ , of  $V(R_\odot) = (239 \pm 5)$  km/s. Adopting these values, for  $R < R_\odot$ , we can transform the available HI disk terminal velocities  $V_T$  into circular velocities  $V(R)$ :  $V(R/R_\odot) = V_T(R/R_\odot) + \frac{R}{R_\odot} V_\odot$  (see McMillan 2011; Nesti and Salucci 2013 and references inside). For  $R > R_\odot$  out to  $\sim 100$  kpc, the MW circular motions are inferred from the kinematics of tracer stars in combination with the Jeans equation (Xue et al. 2008; Brown et al. 2009).<sup>10</sup> In Sofue (2017) the issue of the RC of the MW compared with those of spirals of similar luminosity is discussed.

The mass model of the MW is that of any other spiral: it includes a central bulge, a stellar disk, an extended gaseous disk and all these components are embedded in a spherical dark halo (see Caldwell and Ostriker 1981; Catena and Ullio 2010; Nesti and Salucci 2013; Sofue 2013). As regard to the latter, in a number of studies, the available kinematics is not able to discriminate between the cored and a cusped DM halo profiles (e.g., Catena and Ullio 2010, 2012).

Nesti and Salucci (2013) have alternatively assumed a B-URC and a NFW DM halo profile. They fitted the resulting velocity models to the available kinematical data: HI terminal velocities, circular velocities as recently estimated from maser star forming regions and velocity dispersions of stellar halo tracers in the outermost Galactic regions. They found, for the first model, the following best fit values:  $\rho_0 = 4 \times 10^7 M_\odot/\text{kpc}^3$ ,  $r_0 = 10$  kpc and  $M_D = 6 \times 10^{10} M_\odot$ ,  $M_{\text{vir}} = 1.2 \times 10^{12} M_\odot$  that coincide with those of the URC with the same virial mass and optical radius. The mass model with NFW halo profile fits quite well the dynamical data, however, the resulting best fit value for the concentration parameter  $c$  is:  $c = 20 \pm 2$ , higher than the predicted value from only dark matter  $\Lambda$  CDM simulations. Similar findings were obtained also by Catena and Ullio (2010, 2012); Deason et al. (2012).

### 8.3 Low surface brightness galaxies

There is a limited number of recent studies on the RCs of LSB galaxies, although some of these objects appear in well studied samples of disk systems discussed in the previous sections. In LSB the 21-cm HI line provides us with the main observational channel probing the gravitational field: radio telescopes only now reach sufficient spatial resolution and sensitivity to map small and faint objects like LSB.<sup>11</sup>

Di Paolo and Salucci (2018) applied to LSBs the concept of the stacked analysis of RCs that in spirals has led us to the URC. They investigated, in a sample of 72 objects with available rotation curves and infrared photometry, the distribution of the baryonic and the dark matter components. The galaxies were divided in five velocity bins according to their increasing values of  $V_{\text{opt}}$ . Noticeably, when we plot them in physical units:  $\log V(\log r)$ , they show

<sup>10</sup> The raw kinematical data needed to build the Galaxy RC can be found Pato and Iocco (2017), see Fig. 14.

<sup>11</sup> SKA will exponentially increase the amount of available kinematics.

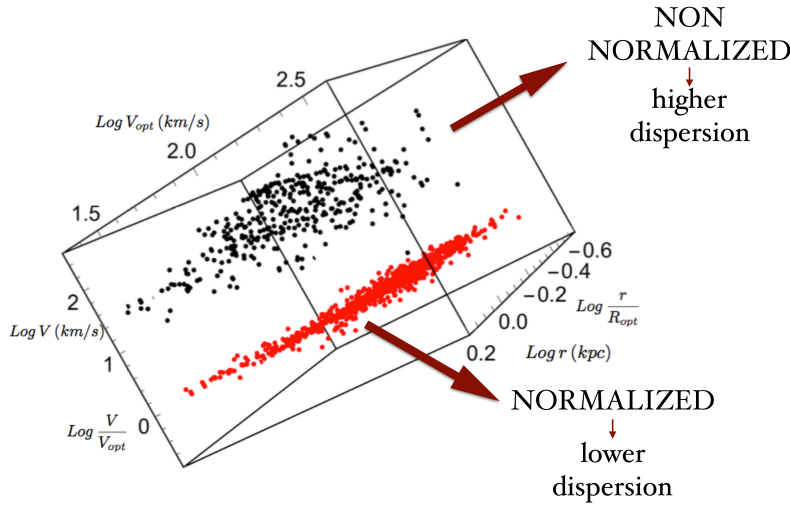


**Fig. 15** The rotation curves of the LSBs sample of Di Paolo and Salucci (2018) in physical (*black*) and normalized units (*red*)

a great diversity: objects with a same maximum velocity possesses very different RC profiles, see Fig. 15. Instead, when we adopt the specifically normalized units:  $x \equiv r/R_{\text{opt}}$  and  $v(x) = V(x)/V(1)$ , the rotation curves  $\log v(\log x)$  of each velocity bin are all alike, see Fig. 15, probing, as in spirals, the idea that by stacking and by coadding diverse RCs, we get a 3D universal profile, i.e., a surface function of  $x$  and of one galaxy structural quantity, e.g.,  $\log V_{\text{opt}}$ . The diversity in the RCs is caused by the presence of another structural parameter in the mass distribution that the stacking processes and the double-normalization neutralize. From the double-normalized velocities, five coadded RCs have been built:  $V_{\text{coadd}}(x, V_{\text{opt}})$ . They are very well fit by the spirals URC velocity profile  $V_{\text{URC}}(x; \rho_0, r_0, M_D)$  (see 41) see Figs. 5–6 of Di Paolo and Salucci (2018).

The resulting URC of LSB galaxies (Fig. 18 of Di Paolo and Salucci 2018) implies that the B-URC halo parameters  $\rho_0$  and  $r_0$  connect with  $R_D$  and  $M_D$  in a way similar to that found in spirals (Di Paolo and Salucci 2018). Moreover, also in these objects we find:  $\rho_0 r_0 \sim 100 M_{\odot} \text{pc}^{-2}$

Remarkably, in LSBs, the URC, expressed in normalized radial units, has *two* independent parameters: one, as in spirals, is the stellar disk or the halo mass, the second is the compactness, either of the dark halo or of the luminous disk; in fact, a tight correlation between these two quantities emerges (without a plausible physical explanation) (see Fig. 28).

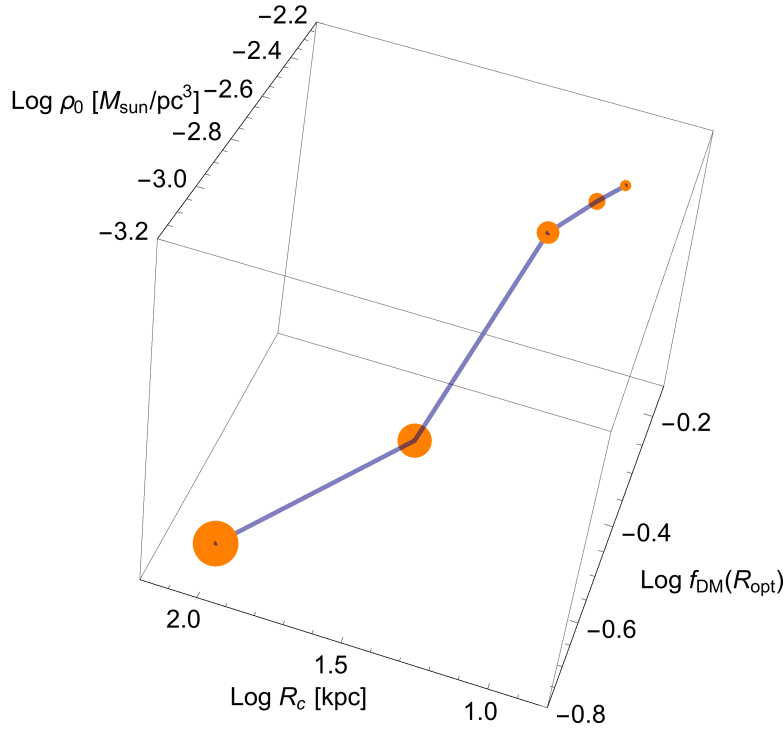


**Fig. 16** The 4D relationship in Fig. 11 (bottom, left) for low-surface-brightness galaxies (Di Paolo and Salucci 2018). Legenda:  $R_c \equiv r_0$ .

#### 8.4 Dwarf disks

Oh et al. (2015) have investigated 26 high-resolution rotation curves of dwarf (irregular) disk (**dd**) galaxies from LITTLE THINGS sample, a high-resolution VLA HI survey of nearby dwarf galaxies. The rotation curves were decomposed into their baryonic and DM contributions in a very accurate way: in these objects, the first component is much less important than the second. Generally, the RCs of **dds** are found to increase with radius out to several disk length scales. Furthermore, the logarithmic inner slopes  $\alpha$  of their DM halo densities are very high:  $\langle \alpha \rangle = -0.32 \pm 0.24$ , in disagreement with the prediction of cusplike NFW halos  $\langle \alpha \rangle_{\text{NFW}} < -1$  (see Fig. 17). This result is confirmed also by the full mass modelling when it is possible to accurately perform it.

Karukes and Salucci (2017) investigated a sample of 36 objects with good quality rotation curve drawn from the Local Volume Sample. They found that, although several objects have a RC suitable for individual mass modelling, on the whole, the stacked analysis yields very important results. They found that, despite variations in luminosities of  $\sim 2$  dex and, above all, despite a great diversity in their rotation curves profiles  $V(R)$ , when radii and velocities are normalized by  $(R_{\text{opt}}, V_{\text{opt}})$  the RCs look all alike (see Fig. 18) and lead to what

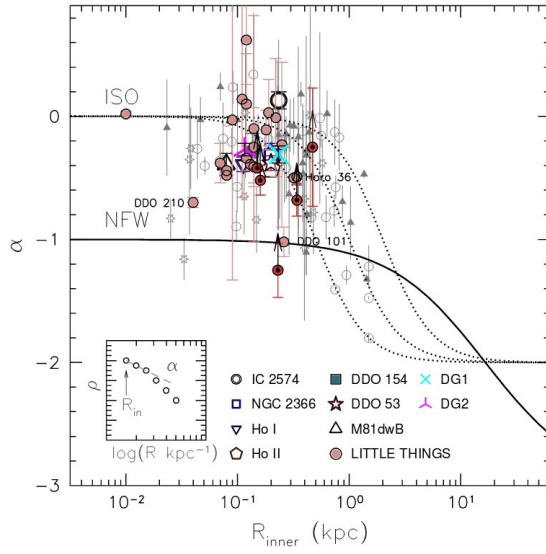


**Fig. 17** The slope  $\alpha$  of the DM density:  $\rho_{\text{DM}} \propto (r/R_{\text{inner}})^\alpha$  with  $R_{\text{inner}}$  the innermost radius with velocity measurement. Also shown the predictions for halos of mass  $10^{10} M_\odot$  and a pseudo-isothermal (ISO) or NFW halo profile. Image reproduced with permission from Oh et al. (2015), copyright by AAS.

can be considered as the low-mass continuation of  $V_{\text{coadd}}(x, M_I)$ , the coadded RCs of spiral galaxies. This finding addresses the “diversity problem” (Oman et al. 2015); it confirms that dwarf disk galaxies, with the same maximum circular velocity, exhibit large differences in their inner RC profiles and then, in their inferred DM densities. However, this pattern disappears when the relevant quantities are expressed in normalized units (see Fig. 18). The reason is that these galaxies have a large scatter in the luminosity vs. size relationship (see Karukes and Salucci (2017)) which, exactly as in LSB, gets neutralised by the normalization procedure performed while building the  $V_{\text{coadd}}$ . Of course the issue itself does not disappear, but it actually thickens and manifests itself as arisen from the strong correlation between the distribution of dark and luminous dark matter and from the presence in these objects of an additional structural quantity: the compactness  $C_\star$  (see later) belonging to the luminous world, but independent, by construction, of the galaxy luminosity (see Karukes and Salucci 2017).

Let us stress that, differently from spirals and LSBs, we need just one  $V_{\text{opt}}$  to represent all **dds** double-normalized RC’s, laying in the range  $10 \text{ km/s} < V_{\text{opt}} < 80 \text{ km/s}$ : in fact, all their (double normalized) velocity profiles are almost identical. The velocity modelling starts from the coadded RC  $V_{\text{coadd}}(R/R_{\text{opt}}, \langle V_{\text{opt}} \rangle)$ , with  $\langle V_{\text{opt}} \rangle = 40 \text{ km/s}$ . As in spirals and LSBs, these data are fitted by the **dd** URC model that includes an exponential Freeman disc, a B-URC DM halo and a gaseous disks. The fit is very successful, unlike that relative to the NFW halo+stellar and gaseous disks velocity model (Karukes and Salucci 2017).



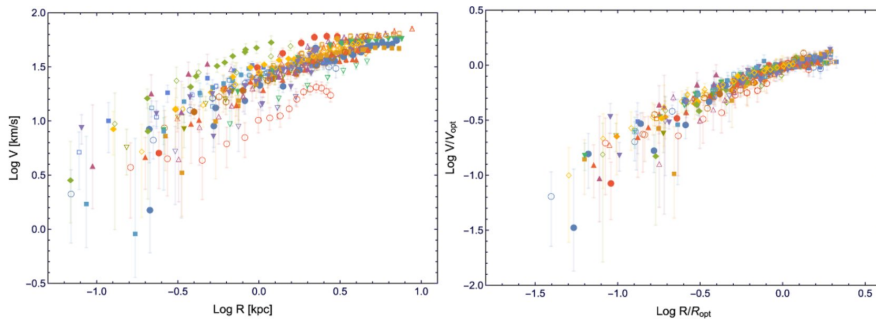


**Fig. 18** dds. The 36 RCs in physical units (*left*) and in two-normalized units (*right*). In Karukes and Salucci (2017) one finds the  $R_{\text{opt}}$  vs.  $L_K$  relationship whose scatter is responsible for the evident diversity of the various RC profiles when they are expressed in physical units. Image reproduced with permission from Karukes and Salucci (2017), copyright by the authors.

These systems are strongly dominated by dark matter halos with cored density profile. The core sizes are proportional to the corresponding disk length scales:  $r_0 = 3 R_D$ , continuing the relationship found in spirals and extending it 2 dex down in galaxy luminosity (Karukes and Salucci 2017). Also, all the other dark and luminous structural properties of the dark and luminous matter, including the stellar/DM compactness  $C_*$  and  $C_{\text{DM}}$ , result amazingly correlated (Karukes and Salucci 2017).

All structural relationships established in normal spirals extend down to “dd” galaxies, the relevant aspect being that also those that connect the dark and the luminous world continue, unchanged, in objects where the dark matter is, by far, the dominant component.

## 9 The distribution of matter in spheroids

Spheroidal galaxies include the biggest and the smallest galaxies of the Universe. The investigation of their dark matter component is rather complicated. With respect to spirals, the bulk of stars in ellipticals is much more compact and then it probes much inner and more luminous matter dominated galactic regions than the stellar and HI disks do in spirals. However, the halos of ellipticals are filled with objects, like planetary nebulae and globular clusters that can be good tracers of the gravitational potential, in spite of their limited number and totally unknown dynamical state.

### 9.1 The fundamental plane in ellipticals

The luminous regions of ellipticals show a 3D relationship, known as the fundamental plane, which is usually written as

$$\log \frac{R_e}{\text{kpc}} = a \log \frac{\sigma}{\text{kms}^{-1}} - \frac{b}{2.5} \frac{\mu_e}{\text{mags}} + c, \quad (43)$$

where  $R_e$  is the effective radius,  $\sigma$  is the central velocity dispersion (corrected to an aperture of  $R_e/8$ ).  $\mu_e$  and  $\log I_e$  are the surface brightness and surface luminosity within  $R_e$ . It is worth to remind that for virialized stable objects, all with the same surface profile  $I(r/R_e)$  and small amount of dark matter inside  $R_e$ , one expects:  $R_e = \sigma_0^a / I_e^b$ , with  $a = 2$  and  $b = 1$ . It is well known that the FP has different parameters (Djorgovski and Davis 1987; Dressler et al. 1987; Jorgensen et al. 1996), e.g.,  $\log R_e = 1.24 \log \sigma_0 - 0.82 \log \langle I \rangle_e$  with scatter 0.07 dex in  $\log R_e$ . As a recent example, Hyde and Bernardi (2009) used a sample of about 50,000 early-type galaxies based on the SDSS-DR4/6, photometric and spectroscopic parameters and obtained  $a = 1.3 \pm 0.05$ ,  $b = 0.3 \pm 0.05$  with r.m.s. of 0.1 dex (See Fig. 19).

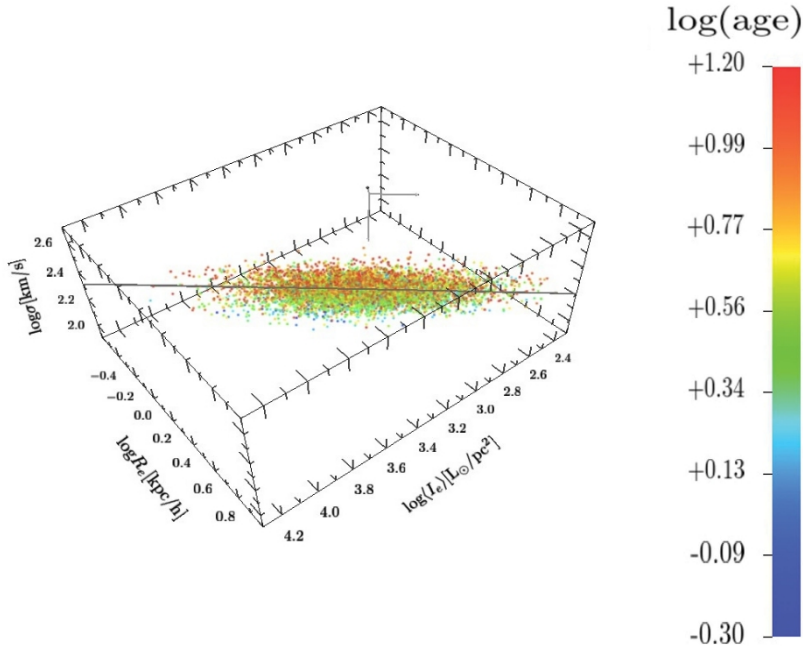


**Fig. 19** The fundamental plane of ellipticals from Hyde and Bernardi (2009) in the coordinate system  $I_e, R_e, \sigma(1/8R_e)$ . Image reproduced with permission from Magoulas et al. (2012), copyright by the authors.

Moreover, Magoulas et al. (2012) investigated the near-infrared FP in  $\sim 10^4$  early-type galaxies (ETG) included in the 6dF Galaxy Survey (6dFGS). They fitted the distribution of central velocity dispersions, near-infrared surface brightness and half-light radii with a three-dimensional Gaussian model that provided an excellent match to the observed properties.

The resulting FP reads as:  $R_e \propto \sigma^{1.52 \pm 0.03} I_e^{-0.89 \pm 0.01}$ , with a r.m.s. of 23%. The deviation of the FP with respect to the theoretical predictions, called the tilt of the FP, has been thought to be due a combination of several

effects (Bernardi et al. 2003; Bolton et al. 2008; Hyde and Bernardi 2009; Graves and Faber 2010 and Zaritsky (2012) for a review). However, from recent independent and accurate measurements of the total mass inside  $R_e$  by means of stellar dynamics (Cappellari et al. 2006; Thomas et al. 2011) and strong lensing (Bolton et al. 2007; Auger et al. 2010), it is clear that variations among ETGs of the stellar mass to light ratio  $M/L$  are the cause of the tilt. This has clearly emerged in Cappellari et al. (2013): they started with the FP which reads as

$$\log\left(\frac{L}{L_{\odot,r}}\right) = a + b \log\left(\frac{\sigma_e}{130 \text{ kms}}\right) + c \log\left(\frac{R_e}{2 \text{ kpc}}\right), \quad (44)$$

$\sigma_e$  and  $R_e$  are normalized to the median values found in sample under study. The resulting values of the parameters are:  $b = 1.25 \pm 0.04$ ;  $c = 0.96 \pm 0.03$  and the r.m.s. scatter is 0.1 dex; when the galaxy luminosity is replaced by the dynamical mass  $L \times (M/L)_{\text{dyn}}$ , obtained by self-consistent JAM modelling (see Sect. 5.5) a smaller r.m.s. it is found and the parameters:  $b = 1.93 \pm 0.03$ ,  $c = 0.96 \pm 0.02$  acquire the virial values. This confirms that a major part of the scatter of the FP is actually due to variations in the  $M/L$ s values.

Therefore, the fundamental plane of ETGs expresses the properties of the virialized stellar spheroids and, differently from the Tully–Fisher in spirals, is not directly related to the properties of DM distribution (inside  $R_e$ ). Finally, this result lends support to the idea, valid in spirals, that the dynamically measured mass is more accurate prior of luminous mass of a galaxy than the luminosity itself.

## 9.2 The dark matter distribution in ellipticals

The derivation of the distribution of dark and luminous mass in ellipticals is far more difficult than in disk systems. The kinematics is more uncertain and the tracers of the gravitational field often do not cover sufficiently well the crucial region between  $1/3 R_e$  and  $3 R_e$  where the system becomes from stellar dominated to DM dominated.

The main issues under investigation are: *a*) an universal power law slope of the *total* density profile:  $\rho_{\text{tot}} \propto r^{-2}$  and *b*) large variations of the  $M_*/L$  ratio with mass and other quantities. As regard to the first issue, let us stress that the above density law in ellipticals and the case  $V(R) = \text{const}$  in spirals are different configurations (see Eq. 19). As regard to the second, at fixed galaxy luminosity, the stellar mass-to-light ratios vary in ellipticals much more than in spirals.

As regard to investigations in early-type galaxies (ETG)s one has to report the several different approaches devised to obtain their mass distribution. However, it is fair to stress that it is difficult to make a synthesis of the results obtained so far, being the situation still in full development.

Data from the Sloan Lens Advanced Camera for Surveys (SLACS) project (Bolton et al. 2006) provided us with the total matter density profiles for a

sample of 73 ETGs with strong lenses and large stellar masses ( $M_* > 10^{11} M_\odot$ ) (Auger et al. 2010). For each galaxy the relevant quantities are the Einstein radius  $R_E$ , its relative enclosed mass, the stellar mass, and  $\sigma_E$  the velocity dispersions at  $R_E$ . An isotropic mass model was assumed and they found: ( $\rho_{\text{tot}}(r) \propto r^{-\gamma}$ ) with  $\langle \gamma \rangle = 2.08 \pm 0.03$  and with a scatter among galaxies of  $\sigma_\gamma = 0.16$ .

Cappellari (2012) determined the total density profile for a sample of 14 ETGs fast-rotators (stellar masses  $10.2 < \log M_*/M_\odot < 11.7$ ). SLUGGS and ATLAS observations provided the 2D stellar kinematics out to about to  $4 R_e$ , reaching the region dominated by dark matter and poorly investigated before. They built axisymmetric dynamical models based on the Jeans equations solved with a spatially varying anisotropy  $\beta$  and a general density profile for the dark matter halo. The resulting *total* density profiles were found to be to follow, from  $R_e/10$  to  $4R_e$ , the the power law:  $\rho_{\text{tot}}(r) \propto r^{-\gamma}$  with  $\langle \gamma \rangle = 2.19 \pm 0.03$ . This extension of the above power law relationship to regions well outside  $R_{1/2} \simeq R_e$  is far than trivial and likely hides a connection between the dark halo and the stellar spheroid.

Tortora et al. (2014) have investigated the central regions ( $r < R_e$ ) of ETGs by using strong lensing data from SPIDER and kinematics and photometric data from ATLAS<sup>3D</sup>. The analysis extends the range of galaxy stellar mass ( $M_*$ ) probed by gravitational lensing down to  $\sim 10^{10} M_\odot$ . Each galaxy was modeled by two components (dark matter halo + stellar spheroid). The following DM halo profiles were considered: NFW, NFW-contracted, and Burkert. The mass-to-light ( $M_*/L$ ) was normalized to the Chabrier IMF as  $M_*/L = \delta_{\text{IMF}}(M_*/L)_{\text{Chabrier}}$  with  $\delta_{\text{IMF}}$  a free parameter describing the systematic variations of IMF among galaxies. They found that, generally: 1)  $\delta_{\text{IMF}}$  increases with galaxy size and mass. 2)  $\alpha(R_e/2) = d \log M/d \log r - 3$  in the most massive ( $M_* \sim 10^{11.5} M_\odot$ ) or largest ( $R_e \sim 15$  kpc) ETGs reaches the value of  $-2$ , while in low-mass ( $M_* \sim 10^{10.2} M_\odot$ ) or very small ( $R_e \sim 0.5$  kpc) ETGs decreases to the value of  $-2.5$ . As regard to the DM distribution, the result of this work could not reach an explicit preference for a particular profile.

Chae (2014) investigated  $\sim 2,000$  nearly spherical Sloan Digital Sky Survey (SDSS) ETGs, at a mean redshift of  $\langle z \rangle = 0.12$  and assembled mass models based on their aperture, velocity dispersions, and luminosity profiles measurements. A two-components mass model (i.e., stellar spheroid plus dark halo) successfully fitted, inside  $R_{1/2}$ , the SDSS aperture velocity dispersions. As result, they confirmed that, in the region:  $0.1 R_{1/2} < R < R_{1/2}$ , the total density (dark halo + stellar spheroid) exhibits a power law behavior:  $\rho_{\text{tot}}(r) \propto r^\gamma$  with  $\langle \gamma \rangle = -2.15 \pm 0.04$ .

Oguri et al. (2014) investigated 161 strong gravitational lenses from SLACS and BELLS and a number of strongly lensed quasars. They derived the stellar mass  $M_*^{\text{Sal}}$  for each lensing galaxy by fitting the observed spectral energy distribution to a stellar population synthesis model with a Salpeter IMF (Bruzual and Charlot 2003). The measurement in these lens galaxies of the sizes of their Einstein rings  $R_E$  allowed them to build normalized total mass profiles for each object:  $M_{\text{tot}}(< R_E)/M_*^{\text{Sal}}$  and to normalize the projected radius  $R$

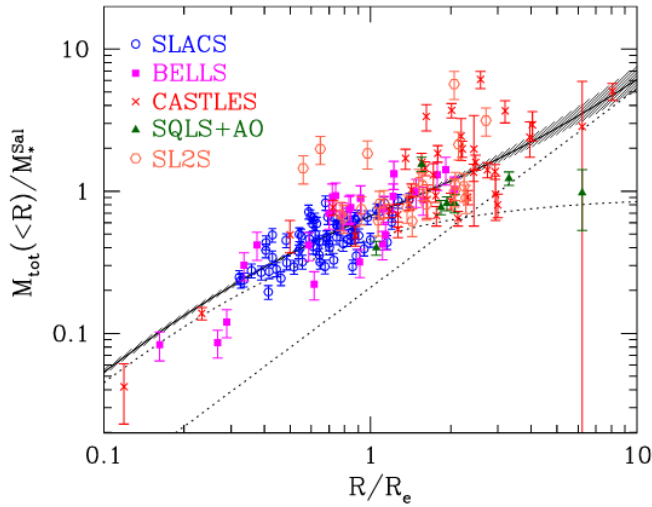


**Fig. 20** Normalized mass of ETGs as function of its normalized radius. Also shown: the best-fit mass profile *solid line* and the stellar spheroid and the power law DM halo contributions *green and red dotted lines*. Image reproduced with permission from Oguri et al. (2014), copyright by the authors.

by the effective luminosity radius  $R_e$ . Notice that this double-normalization is of the same kind of that performed in the **dd** galaxies (Karukes and Salucci 2017). They derived, from each Einstein ring, the relative scaled mass profile  $M_{\text{tot}}(<R_E/R_e)/M_*^{\text{Sal}}$ . These data were fitted by the model

$$\frac{M_{\text{tot}}(<R)}{M_*^{\text{Sal}}} = A \left( \frac{R}{R_e} \right)^{3+\gamma}. \quad (45)$$

They found  $\gamma = -2.11 \pm 0.05$ . Furthermore, they decomposed the total mass in its dark and luminous components: a power-law spherical DM dark halo and a Hernquist spheroid for which, with  $y \equiv R/R_e$ :  $M_{\text{Her}}(y) = M_{\text{sph}} y^2 / (1.4^2 + y^2)$

$$\frac{M_{\text{DM}}(<R)}{M_*^{\text{Sal}}} = A_{\text{DM}} \left( \frac{R}{R_e} \right)^{3+\gamma_{\text{DM}}}. \quad (46)$$

Quasar microlensing measurements break the IMF-stellar mass degeneracy, the DM fraction inside  $R_e$  results:  $A_{\text{DM}}/A = 0.2$  and  $\gamma_{\text{DM}} = -1.60^{+0.18}_{-0.13}$  that implies that DM is distributed in a way shallower than the total matter, as it occurs in disk systems, see Fig. 20.

Poci et al. (2017) (see also Cappellari et al. 2013), by modelling kinematical and photometric data of 258 early-type galaxies, belonging to the volume-limited ATLAS<sup>3D</sup> survey, derived their density profiles and found the usual power law:  $\rho_{\text{tot}}(r) = r^\gamma$  with  $\gamma = -2.2 \pm 0.2$ . Noticeably, however, they did find significant variations of  $\gamma$  with  $\Sigma_e$  the surface brightness inside  $R_e$  and  $\sigma_e$ , in some contrast with previous works.

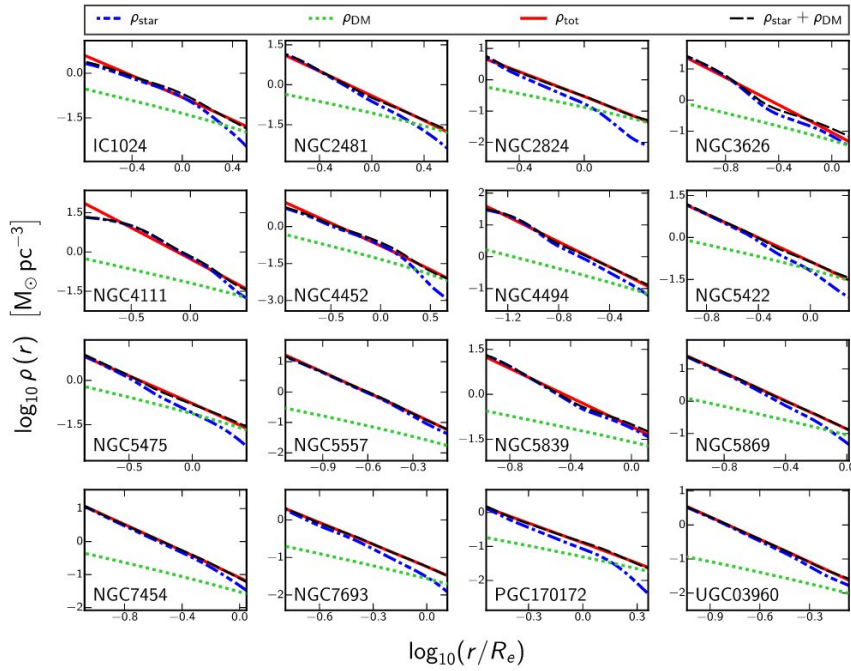


**Fig. 21** The total density profile *solid line* and its stellar *dotted line* and DM *dot-dashed line* components for 16 galaxies from the ATLAS survey. Image reproduced with permission from Poci et al. (2017), copyright by the authors.

Serra et al. (2016) investigating a sample of 16 fast-rotator ETGs with HI disks extended out to  $\sim 6 R_e$  established a tight linear relation between  $V_{\text{HI}}$  the (flat) circular velocity measured from resolved HI observations in (external) DM dominated regions (i.e., for  $R \gg R_e$ ) and  $\sigma_e$ , the velocity dispersion measured at  $R_e$ , i.e., in a luminous matter dominated region:

$$V_{\text{HI}} = 1.33\sigma_e, \quad (47)$$

with an observed scatter of 12 percent. The tightness of the correlation suggests a strong coupling between luminous and dark matter, analogous to the situation in spirals, in LSBs and in **dds**. Eq. (47) implies a decline in the effective circular velocities  $V(r)$  from  $R_e$  to the outer regions. Such drop is in excellent agreement with the results of Cappellari et al. (2015) and, remarkably, is similar to that observed in early-type spirals (Noordermeer et al. 2007) and in the most luminous late type spirals (Salucci et al. 2007). Assuming  $\rho_{\text{tot}}(r) \propto r^{-\gamma}$ , Eq. (47) implies  $\langle \gamma \rangle = 2.18 \pm 0.03$  across the sample, with a scatter of 0.11 around the average value (see Fig. 22).

Alabi et al. (2018) (see also Alabi et al. 2016) used globular cluster kinematics data, primarily from the SLUGGS survey, to measure the dark matter fraction  $f_{\text{DM}}(5 R_e)$  and the average dark matter density  $\rho_{\text{DM}}(5 R_e)$  within  $5 R_e$  for 32 nearby ETGs with stellar mass  $\log(M_*/M_\odot)$  ranging from 10.1 to

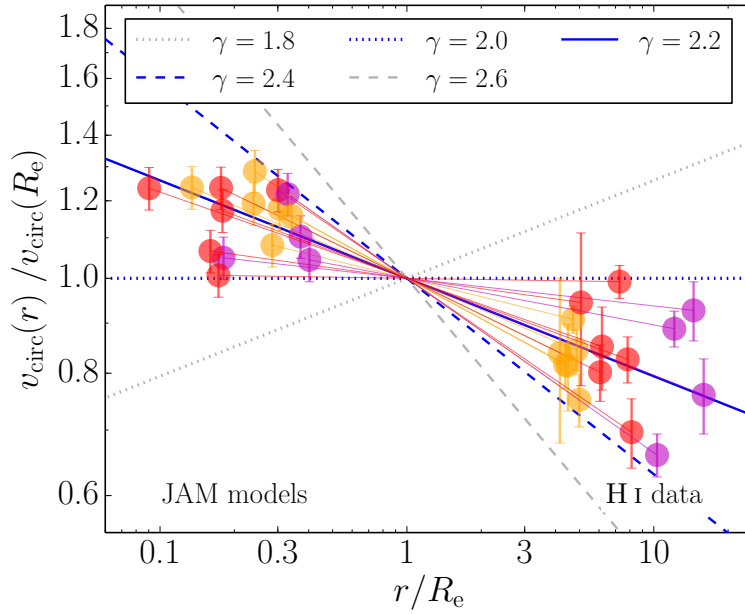


**Fig. 22** Radial profile of the normalized circular velocity for the sample of ellipticals in Serra et al. (2016). Data come from JAM models for  $R < R_e$  and from HI 21 cm for  $R > R_e$ . Points and solid lines are coded according to the increasing  $R_{\text{HI}}/R_e$  ratio.

11.8. They found that  $f_{\text{DM}}(R_e) \sim 0.6$  for galaxies with stellar mass lesser than  $(M_*/M_\odot) \sim 10^{11}$ . At higher masses, a sudden large range of  $f_{\text{DM}}(R_e)$  values emerges. This seems in contradiction with the total density power law  $\rho_{\text{tot}} \propto r^{-2.1 \pm 0.1}$  usually found in other determinations.

Pulsoni et al. (2017) used planetary nebulae (PNe) as tracers of the gravitational field around ellipticals. They obtained two-dimensional velocity and velocity dispersion for 33 ETGs. The velocity fields were reconstructed from the measured PNe velocities. The data extend out from  $3R_e$  to  $13R_e$ . The objects show a kinematic transition between the inner luminous matter dominated regions and the outer halo dominated ones. These transition radii, in units of  $R_e$ , anti-correlate with stellar mass, differently from what occurs in spirals. The galaxies appear to have more diverse kinematic properties in their halos than in their central regions. It is noticeable the fact that 15% of the galaxies in the sample have steeply falling profiles implying that, inside  $R_e$ , the fraction of dark matter is very negligible.

One important issue of the ETGs is the comparison between the  $M/L$ 's inferred from their dynamical or strong lensing modelling and those inferred from the fitting of their spectral energy distributions. Cappellari (2016) have investigated it with a large sample of objects. The values derived, see Fig. 23), indicate the existence of random variations of the IMF and variations with the galaxy dispersion velocity. Noticeably, the existence of a non universal initial

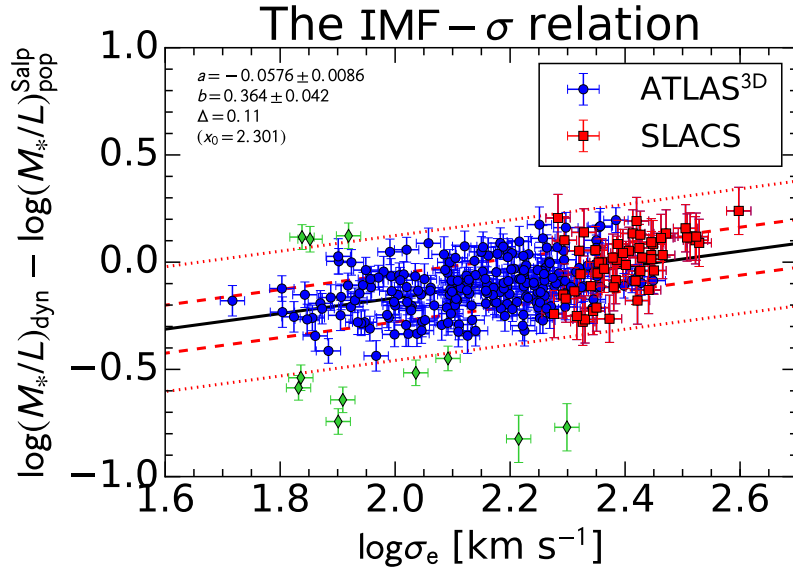


**Fig. 23** The mass discrepancy– $\sigma$  relation, very likely created by systematical variations of the IMF among ETGs (see Cappellari (2016); Posacki et al. (2015)).

mass function (IMF) is already present at intermediate redshift (Tortora et al. 2018).

Evidences that ellipticals have variable IMF them come Also from their chemical evolution model reproducing the abundance patterns observed in the sample of the Sloan Digital Sky Survey Data Release 4 (De Masi et al. 2018). The model assumes ellipticals form by fast gas accretion, and suffer a strong burst of star formation followed by a galactic wind, which quenches star formation. The model if assumes a fixed initial mass function (IMF) in all galaxies, fail in simultaneously reproducing the observed trends of chemistry with the galactic mass; only a varying IMF among ellipticals, leads to an agreement with data.

Corsini et al. (2017) have investigated NGC 7113, and PGC 67207, two bright ETGs in low-density environments. These rare objects may help us disentangling in ellipticals what is of pertinence of the process of their formation and what is inherent to the properties of their dark matter halos. The surface-brightness distributions and their parameters were derived by  $K_S$ -ugriz-band two-dimensional photometric decomposition. The line-of-sight stellar velocity distributions inside  $R_e$  were measured along several position angles. They assumed the BT-URC DM halo profile (see Eq. 29). The luminous and dark distributions were obtained from the orbit-based axisymmetric dynamical modelling (see Sect. 5.5). The fit model to the data is excellent and implies that these galaxies have a lower content of dark matter with respect to early-type galaxies living in high-density environments. Moreover, it is important to no-



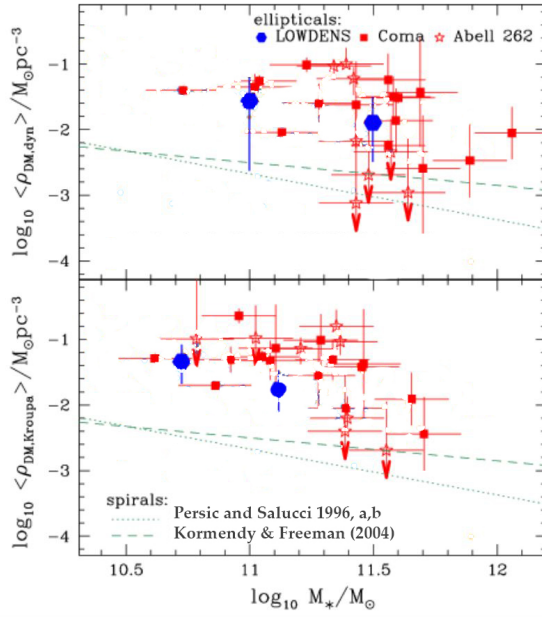


**Fig. 24** The average density inside  $2R_e$  in NGC 7113 and PGC 67207 (blue hexagons as a function of their stellar spheroid mass  $M_*$  computed a) dynamically (*top*) or b) from the photometry (*bottom*). Also shown the values for ETGs in Coma Cluster (*red filled*) and in Abell 262 (*red open*). The lines show the corresponding spirals' relationship. Image reproduced with permission from Corsini et al. (2017), copyright by the authors.

tice that their DM density inside  $2R_e$  is significantly higher than in similar mass spirals (see Fig. 24).

### 9.3 DM in dwarf spheroidals

Dwarf spheroidal (dSph) galaxies are the smallest and least luminous galaxies in the Universe and provide unique hints on the nature of DM. They are old, in dynamical equilibrium and with no HI component. They contain a (small) number of stars, which provide us with tracers of the gravitational field. The very negligible baryonic content that they show does not affect their mass modelling and it also indicates that this component may have never modified the primordial DM distribution (see Walker (2013)) Then, by investigating these galaxies, we probe the original structure of the DM halos (see the review of Battaglia et al. 2013).

The stellar component for each dwarf spheroidal galaxy is modeled by means of a Plummer density profile with its scale radius  $R_e$ , see Eq. (12). The main sample includes the eight larger dSphs of the Milky Way: Carina, Draco, Fornax, Leo I, Leo II, Sculptor, Sextans, and Ursa Minor. The determination of the DM mass profile  $M(r)$  requires the velocity dispersion profile along the

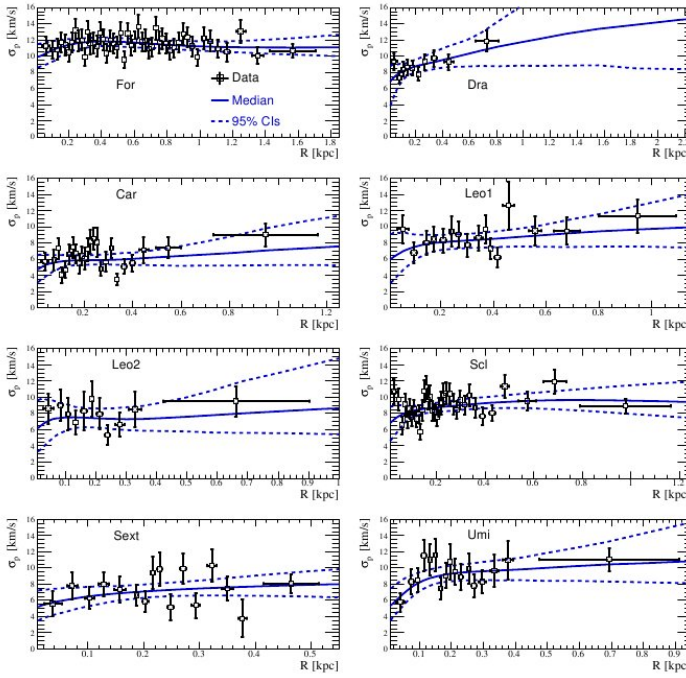


**Fig. 25** Line-of-sight dispersion velocities of the “classical” dSphs. A large r.m.s. is evident. Image reproduced with permission from Bonnavard et al. (2015), copyright by the authors.

line-of-sight  $\sigma_{\text{l.o.s.}}(r)$  (see Fig. 25). The very limited number of these galaxies combined with the large range in the values of their physical quantities make the stacked analysis approach impossible for investigating the dSphs mass distribution. There are three common methods that use available observations to infer the DM density profile in dSphs.

*Jeans analysis:* In this approach one feeds Eq. (18) with the values of  $\nu_*(R)$ , the stellar density profile, uses a large number of well determined dispersion velocities  $\sigma_{\text{l.o.s.}}(r)$  (Walker et al. 2009a) and assumes a particular anisotropy profile (e.g., as in Bonnavard et al. 2015). Then, through a Monte Carlo analysis, one obtains the free parameters of the DM density profile  $\rho(r)$  and the anisotropy function  $\beta$ . There are views that this investigation, also when the tangential velocity dispersions are available, cannot resolve in these objects the cusp/core issue (Walker et al. 2009b; Strigari et al. 2008; Bonnavard et al. 2015; Strigari et al. 2018). The degeneracy in the Jeans equation between the mass and the anisotropy profiles, combined with a kinematics of limited extension and quality, makes difficult to determine the density profile by means of this method.

*Slope method:* Walker and Penarrubia (2011) first exploited the fact that in some dSphs there are multiple stellar populations, photometrically and chemo-

dynamically distinct sub-components. They independently trace the (same) gravitational potential. Since  $M(R_e)$ , the mass contained within the effective radius  $R_e$  of each component, can be measured independently of their stellar orbital anisotropies, see Eq. (20) then, we can derive the quantity  $\frac{d \log M}{d \log R}$  at different radii without adopting a DM halo profile. The method, applied to the dSph Fornax and Sculptor, for which two separate stellar sub-components have been disentangled, gives  $\Delta \log M / \Delta \log r = 2.61_{-0.37}^{+0.43}$  and  $2.95_{-0.39}^{+0.51}$ , respectively, pointing to DM densities that keep an almost constant value within the central few-hundred parsecs of these objects. With the same method, Breddels et al. (2013) found that a NFW profile is only marginally allowed in Sculptor.

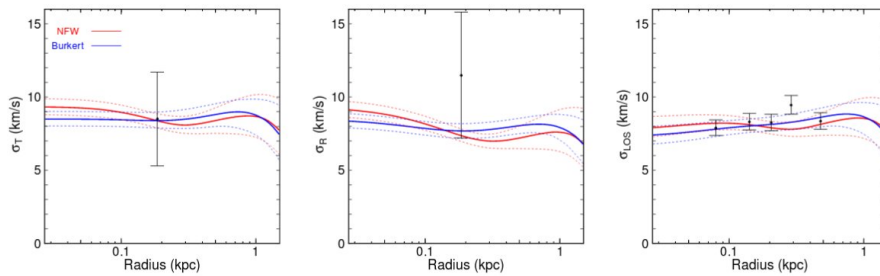


**Fig. 26** Observed versus predicted dispersion velocities from different halo density profiles. Image reproduced with permission from Strigari et al. (2018), copyright by AAS.

This method has been carefully investigated by Strigari et al. (2018) in view of determining the level of its intrinsic bias, see Fig. 26 and finding improvements.

*Schwarzschild modelling:* A promising method, based on distribution functions that depends on the action integrals, has been put forward by Pascale et al. (2018). This was applied to the Fornax galaxy, finding strong evidence for the presence of a cored density profile.

## 10 The LM/DM universal properties

One could resume the state of the art of the issue of “DM in galaxies”, by stressing the unexpected scheme shown by the distributions of the dark and luminous matter in galaxies: halo masses, stellar component/baryonic masses, central densities, luminosities, DM density length scales, half-light radii, and galaxy morphologies are all engaged in a series of relationships, difficult to be understood in a physical sense. However, since the concurrent view argues that “galaxy formation is a complex phenomenon which could account for the apparently inexplicable observational scenario”, we stress that the above is far

beyond a list of galaxy relationships, but a coherent pattern that can help us in the search of the unknown dark particle.

In disk systems (dwarf disks, low surface brightness galaxies and spirals) when the values of their structural quantities are expressed in physical units, the stellar component forms a family ruled by three parameters: the disk length-scale  $R_D$  and the magnitude (e.g.,  $M_I$ ) and the stellar disk concentration  $C_*$ . In the same systems, also the dark component is represented by a family ruled by three parameters: the core radius  $r_0$ , the central density  $\rho_0$  and  $C_{DM}$  the DM concentration. The two families are closely and mysteriously related: the entanglement is so deep that it is difficult to understand which rules which.

Remarkably, the situation much simplifies when we express the circular velocity  $V(r)$ <sup>12</sup> in the double-normalized form:  $V(r/R_{opt})/V(R_{opt})$ . The profiles of the RCs emerge as a function of just one parameter, at choice among the above six, plus  $V_{opt}$ ,  $M_{vir}$  and the angular momentum for unit mass  $j$  (see Lapi et al. 2018). Remarkably, this occurs independently on whether a galaxy is dark matter or luminous matter dominated for  $R < R_{opt}$ . The emerging evidence is that structural quantities deeply rooted in the luminous sector, like the disk length scales, tightly correlate with structural quantities deeply rooted in the dark sector, like the DM halo core radii.

Let us conclude this section noticing that this scenario is, instead, still under investigation in spheroidal galaxies.

### 10.1 The cored distributions of dark matter halos around galaxies

The current situation is the following: a) in disk systems of all *morphologies and luminosities* there is strong evidence that the DM halo density profile is very shallow out to the edge of the stellar distribution  $R_{opt}$  b) in dwarf spheroidals and in ellipticals, also due to the intrinsic difficulty in these systems to disentangle the actual kinematics from the biased one, the situation is less clear, although, also in these objects, there are several claims of cored DM halo density profiles. In conclusion, the claim that DM around galaxies have a density distribution well represented by the cored B-URC profile is bald, but I believe correct.

The most intriguing aspect of the DM in galaxies is not that they all possess a universal density profile, but that, this latter comes with a couple of very unexpected properties. The analysis of rotation curves, dispersion velocities, and weak-lensing data of large samples of dSphs, dwarf irregulars, spirals, and elliptical galaxies, found that the product of the DM core radius  $r_0$  with the DM central density  $\rho_0$  is nearly constant in galaxies, i.e., independent of their luminosity (Donato et al. 2009; see also Donato et al. 2004). This result, pioneered by Kormendy and Freeman (2004), is obtained in Donato et al. (2009) from the mass models derived from 1) about 1000 coadded RCs of

<sup>12</sup>  $V(r) = (r d\Phi/dr)^{1/2}$  with  $\Phi$  the *total* gravitational potential.

spirals, 2) hundredths individual RCs of normal spirals of late and early types 3) galaxy-galaxy weak lensing signals 4) the inner kinematics of Local Group dwarf spheroidals 5) the RCs of 36 **dd** and 72 LSBs (see Di Paolo and Salucci 2018). The relationship reads (see Fig. 27)

$$\log(r_0\rho_0) = 2.15 \pm 0.2, \quad (48)$$

in units of  $\log(M_\odot/\text{pc}^2)$ .

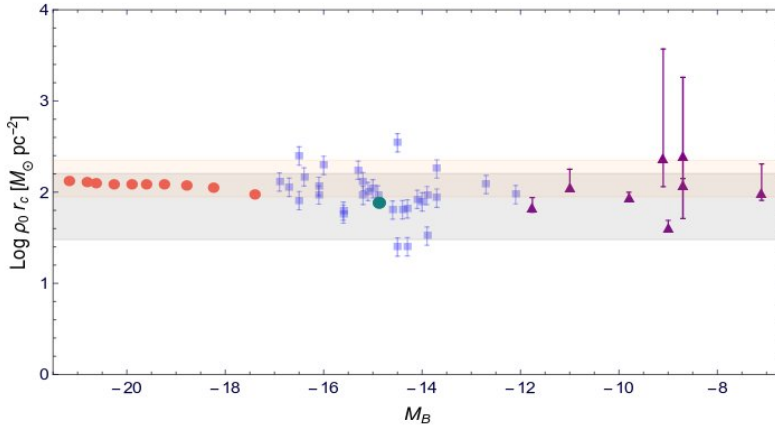


**Fig. 27** (Central DM halo density)  $\times$  (halo core radius) as a function of a galaxy magnitude. Legenda:  $r_c \equiv r_0$ . Data are from the URC of spirals (*red circles*), the scaling relation in Donato et al. (2009) (*orange area*), the Milky Way dSphs (*purple triangles*) Salucci et al. (2012), the **dds** (*blue squares*) Karukes and Salucci (2017). Also shown the relationship by Burkert (2015):  $\rho_0 r_c = 75^{+85}_{-45} M_\odot \text{pc}^{-2}$  (*grey area*) (see also Spano et al. 2008). Image reproduced with permission from Karukes and Salucci (2017), copyright by the authors.

This relationship between the two structural quantities of the DM halos is found in galactic systems spanning over 14 magnitudes and it exploits mass profiles determined by several independent methods. In the same objects, the constancy of  $\rho_0 r_0$  is in sharp contrast with the systematic variations, by about 5 orders of magnitude, of all the other DM-related galaxy quantities, including the central DM density  $\rho_0$  and many of the LM-related galaxy properties, as the magnitude.

At a higher level there is the correlation between the compactness of the stellar disks and that of the DM halos in dark matter dominated **dds** and LSBs (see Fig. 28 and the related caption). It is legitimate to interpret all this as an evidence of the dark and luminous worlds conjuring in galaxies.

The relationship between the halo mass and the stellar mass located at its center is an important and well investigated one. It is well known that the mass fraction  $\frac{DM}{LM}$  as a function of the halo mass follows a characteristic U-shaped curve (Wolf et al. 2010; Moster et al. 2010) for which  $M_{\text{vir}}/M_\star$  is minimized at the halo mass  $M_{\text{vir,break}} \approx 3 \times 10^{11} M_\odot$  and rises at both lower

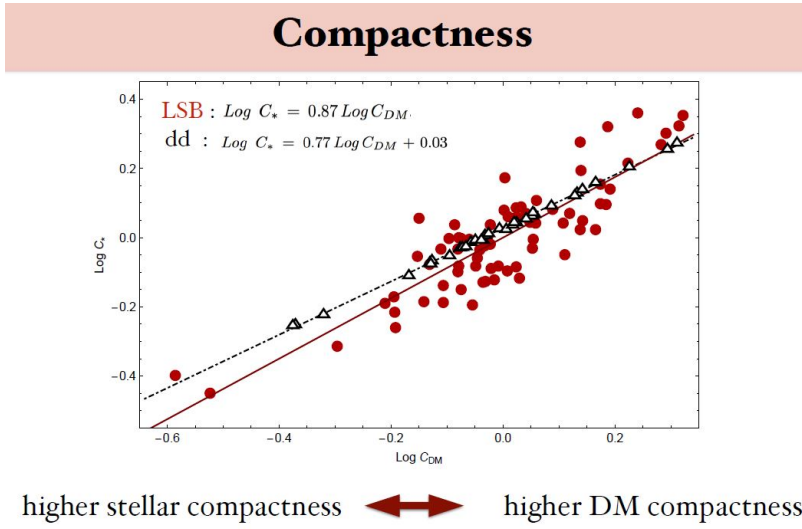


**Fig. 28** The relationships between the compactness of the stellar disks and that of DM halos in *dd* and LSB galaxies (Karukes and Salucci 2017; Di Paolo and Salucci 2018). Let us set:  $\mathbf{M}$  and  $\mathbf{S}$  for a generic galaxy mass and size. We perform, in a sample of galaxies, the regression  $\log \mathbf{S} = a + b \log \mathbf{M}$ . For each galaxy  $i$  of the sample the compactness  $\log \mathbf{C}_i$  is defined by  $\log \mathbf{C}_i = -\log(\mathbf{S}_i) + a + b \log \mathbf{M}_i$ . Here, for the luminous matter:  $\mathbf{M} \equiv M_*$ ,  $\mathbf{S} \equiv R_D$  and  $\mathbf{C}_i \equiv C_*$ ; for the DM:  $\mathbf{M} \equiv M_{\text{vir}}$ ,  $\mathbf{S} \equiv r_0$  and  $\mathbf{C}_i \equiv C_{\text{DM}}$ .

and higher masses. According to the URC, the value of  $M_{\text{vir,break}}$  corresponds to  $M_{\text{star,break}} \sim 1.2 \times 10^{10} M_\odot$  and to  $L_{\text{break}} \sim 5 \times 10^9 L_\odot$  in the  $r^*$ -band luminosity (see also Lapi et al. 2018). Outliers of this relationship do exist (Beasley et al. 2016), however, here we do not further enter this topic certainly related to the “galaxy formation process”.

Therefore, the empirical scenario includes six quantities that define a galaxy: three in the dark sector (halo mass and core radius and DM halo compactness) and three in the luminous sector (stellar/baryonic mass, half-light radius and stellar disk compactness). They all relate each other but, while some of these relationships lay in the heart of the DM mystery, others, instead, lay in the ball-park of the galaxy formation and evolution process.

## 10.2 The dark-luminous matter coupling 2.0

In spirals, dwarf disks and LSBs there are extraordinary multiple connections between the dark and the luminous components. This occurs over many orders of magnitudes in halo masses and over the whole ranges of galaxies morphology and luminosity. The “standard” explanation relates to a dynamical evolution of the galaxies, in particular, of their DM halo densities, caused by powerful baryonic feedbacks. Although this scenario is far than being rejected, it seems, however, unable to cope with the intriguing wealth of correlations between quantities deep-rooted in opposite dark/luminous worlds that we have

presented in this review. More in detail, while we cannot completely rule out the possibility that astrophysical phenomena can be responsible for the above intriguing scenario, on the other hand, what emerges in galaxies allow us to propose a shift of paradigm, according to which, the nature of dark matter is not given to us by convincing theoretical arguments, but must be searched in the various properties of the DM halos and stellar disks.

In Salucci and Turini (2017), it is argued that these new ideas can be justified also by some direct hint: in spirals the DM pseudo pressure  $\rho_{\text{DM}}(r)V^2(r)$  reaches a maximum value always close to the core radius  $r_0$  and this maximum takes the same value in all objects, no matter the galaxy mass. Moreover, at  $r = r_0$  in all disk systems, the quantity  $\rho(r)\rho_*(r)$  takes the same value. We notice that this density product is proportional to the interaction probability between the , the luminous and the dark matter. This is hardly a coincidence, in that, the quantity like  $K_{\text{SA}} = \rho_{\text{DM}}^2(r)$ , which is proportional to the self interaction of the DM component, is largely varying in galaxies and among galaxies. One can speculate that the structure of the inner parts of the galaxies is driven by a direct interaction between dark and luminous components on timescales of the order of the age of the Universe. The DM central cusp, outcome of the proto-halo virialization, as time goes by, gets progressively eaten up/absorbed by the dominant luminous component. The interaction, then, flattens the density of DM and drops the pressure towards the center of the galaxy and it is likely to leave in inheritance the above galaxy relationships.

## 11 Conclusions

On the fundamental issue of dark matter in galaxies there is a substantial difference between spheroidals and disk systems. Let us notice that also the latter statement shows that, although we are focused on DM halos, nonetheless, we must discuss galaxy morphology. And this has been the leitmotiv of this review: the DM component enters in aspects apparently of pertinence of the luminous matter and vice versa.

We have started to point out that the luminosity or a reference velocity is the tag that defines the dark and luminous mass distribution in galaxies. However, very recent results have proven that in spirals, “dd” and LSBs, the universal rotation curve, when expressed in physical units, needs two statistically independent controlling parameters: the luminosity and the compactness. It must be specified that we are not just flagging some empirical relationships: we have three structural properties of the stellar discs that enter in close relation with the three structural properties of the DM halos.

In elliptical galaxies, the situation is still very open. They also show regularities in their total mass distributions: its logarithmic derivative from  $r = 0$  to  $r = R_e$  and beyond is very near to 1, despite that in this region the galaxies pass from a totally LM dominated regime to one with a relevant fraction of dark matter. The fundamental plane of ellipticals and S0 entangles two quantities of the luminous world, the luminosity/stellar spheroidal mass, and

the half-light ratio and a hybrid one: the dispersion velocity, which is rooted in both luminous and dark worlds. Universality in the distribution of matter in ellipticals has not been established yet. We believe that this is due to the insufficient quality and quantity of proper and useful probes of their gravitational potentials. We also have to notice that also for these systems there are evidences of cored DM distributions.

Dwarf spheroidals, despite their limited number, are becoming always more crucial in the investigation of dark matter. Each of these dark spheres, lying at the lowest mass boundary of the cosmological structures harboring stars, is a wealth of information on the dark particle. Unfortunately, we can probe their gravitational field only very near to their centers, with tracers that provide data that are difficult to be unambiguously interpreted. It is worth saying, however, that also for this population of galaxies, there are evidences of cored DM halos with properties similar to those of the disk systems and ellipticals.

The non-gravitational nature of DM remains a mystery (Bertone 2010; de Swart et al. 2017). It seems impossible to explain the observational evidences gathered so far in a simple dark matter framework. In my opinion, they are portals to the new physics that seems to lurk behind the phenomenon called “dark matter”. I think that it will be important to recognize our prejudices and confront them head on, also if this means to end our fascination with the  $\Lambda$  CDM Weakly Interacting Massive Particles scenario.

## 12 Future directions

As a consequence of the reverse-engineering approach to the mystery of the dark matter in galaxies that I advocate here, the future is the past. Namely, I argue that, in the observational properties of galaxies, there is much of the required information to solve the riddle. Unfortunately, we have recovered only a very small part of it, not because it is difficult or long to do, but because we were stuck in a different paradigm where, honestly, all this phenomenology is not so important.

However, the situation is extremely positive because, in the near future, from Gaia to SKA, we will be submerged by an enormous flux of information, coming from different messengers, on all aspects of galaxies, independently if one believes or not that this will lead to a solution of the old mystery of dark matter.

**Acknowledgements** I thank Francesca Matteucci for motivating me towards the enterprise of writing this review. I thank N. Turini, V. Gammaldi, F. Nesti, M. Cobal, A. Bressan, M. Cappellari, G. Danese, A. Lapi, C. Frenk, C. Baccigalupi, A. Pillepich, M.F. de Laurentis, R. Valdarnini and C. di Paolo for very useful discussions. I thank Brigitte Greinoecker for help in the process of writing this review.

## References

Adams JJ, Simon JD, Fabricius MH, et al (2014) *ApJ*, 789:63



- Adhikari R, Agostini M, Ky NA, et al (2017) JCAP 1:025  
Alabi AB, Forbes DA, Romanowsky AJ, et al (2016) MNRAS, 460, 3838  
Alabi A, Ferré-Mateu A, Romanowsky AJ, et al (2018) ArXiv e-print arXiv:1801.09686  
An JH, and Evans NW (2011) MNRAS, 413:1744  
Aprile E, Aalbers J, Agostini F, et al [XENON Collaboration] (2018) PRL 121:111302  
Arcadi G, Dutra M, Ghosh P et al, EPJC, 78:203  
Auger M W et al (2010) ApJ, 724:511  
Bacon R, Copin Y, Monnet G, et al (2001) MNRAS, 326:23  
Bahcall JN (1984) ApJ, 276:169  
Bartelmann M and Maturi M (2016) ArXiv e-print arXiv:1612.06535  
Battaglia G, Helmi A, Breddels M (2013) New Astron Rev, 57:52  
Beasley MA, Romanowsky AJ, Pota V, et al (2016) ApJL 819:L20  
Bell EF, McIntosh DH, Katz N, and Weinberg MD (2003) ApJS 149:289  
Bell E and de Jong RS (2001) ApJ, 550:212  
Bellazzini B, Cliche M and Tanedo P (2013) PRD 88:083506  
Bernal N, Heikinheimo, N Tenkanen T et al, (2017) IJMPA 32:27  
Bernardi M, Sheth RK, Annis J et al (2003) AJ 125:1866  
Bershady MA, Verheijen, MAW, Westfall, KB et al (2010a) ApJ 716:234  
Bershady MA, Verheijen MAW, Swaters RA et al (2010b) ApJ 716:198  
Bertone G (ed) (2010) Particle Dark Matter: Observations, Models and Searches. Cambridge, CUP  
Bertone G and Hooper D (2016) ArXiv e-prints arXiv:1605.04909  
Binney J and Tremaine S (2008) Galactic Dynamics, Princeton, PUP  
Bloom JV et al MNRAS (2017) 472:1809  
Boddy KK, Feng JL, Manoj Kaplinghat M et al (2014) PRD 89:115017  
Bode P, Ostriker JP, Turok N (2001) ApJ 556:93  
Bottema R and Pestaña JLG (2015) MNRAS 448:2566  
Boyarsky A, Nevalainen J, Ruchayskiy O (2007) A&A 471:51  
Brook CB, Santos-Santos I, and Stinson, G (2016) MNRAS 459:638  
Bolton AS, Burles S, Koopmans LVE et al (2006) ApJ 638:703  
Bolton AS et al (2008) ApJ 684:248  
Bolton AS, Burles S, Treu T et al (2007) ApJ 665:105  
Bonnivard V et al (2015) MNRAS, 453:849  
Bosma A (1981a) AJ 86:1791  
Bosma A (1981b) AJ 86:1825  
Bothun GD, Impey CD and Malin DF (1991) ApJ, 376:404  
Breddels MA, Helmi A, van den Bosch RCE et al (2013) MNRAS 433:3173  
Bringmann T et al (2016) PRD 94:103529  
Brown WR, Geller MJ, Kenyon SJ and Diaferio A (2009) ApJ 690:1639  
Bruzual G and Charlot S (2003) MNRAS 344:1000  
Bullock JS and Boylan-Kolchin M (2017) ARAA 55:343  
Burkert A (1995) ApJL 447, L25  
Burkert A (2015) ApJ 808:158  
Butler J (2018) PoS(ALPS2018)030  
Caldwell JAR and Ostriker JP (1981) ApJ 251:61  
Campbell et al (2017) MNRAS 469:2335  
Cappellari M, Emsellem E, Krajnović D et al (2011) MNRAS 413:813  
Cappellari M et al (2012) Nature 484:485  
Cappellari M, Romanowsky AJ, Brodie, JP et al (2015) ApJL 804:L21  
Cappellari M (2016) ARAA 54 597  
Cappellari, M et al (2013) MNRAS 432:1709  
Cappellari, M et al (2006) MNRAS 366:1126  
Carignan, C, and Freeman, KC (1985) ApJ 294:494  
Catena R, and Ullio P (2010) JCAP 08(2010):004  
Catena R and Ullio P (2012) JCAP 05(2012):005  
Catinella B, Giovanelli R and Haynes MP (2006) ApJ 640:751  
Chae K-H (2014) ApJL 788:L15  
Coccatto L, Gerhard O, Arnaboldi M et al MNRAS (2009) 394:1249

- Corbelli E and Salucci P (2000) MNRAS 311:441  
Corsini EM, Wegner GA, Thomas J et al (2017) MNRAS 466:974  
Courteau S (1997) AJ 114:2402  
Cretton N, de Zeeuw PT, van der Marel RP and Rix H-W (1999) ApJS 124:383  
Deason AJ, Belokurov V, Evans NW, An J (2012) MNRAS 424:L44  
de Blok WJG, McGaugh SS and Rubin VC (2001) AJ 122:2396  
de Blok WJG, Walter F, Brinks E et al (2008) AJ 136:2648  
de Blok WJG (2010) Adv Astron 2010:789293  
De Masi C, Matteucci F, and Vincenzo F (2018) MNRAS 474:5259  
de Zeeuw PT, Bureau M, Emsellem E et al (2002) MNRAS 329:513  
Destri C, de Vega P, Sanchez NG (2013) PRD 88:3512  
de Swart J, Bertone G, van Dongen J (2017) Nature Astron 1:005  
de Vega HJ and Sanchez NG (2017) EPJC 77:1  
Di Cintio A, Brook CB, Dutton AA et al (2014) MNRAS 441:2986  
Di Paolo C and Salucci P (2018) ArXiv e-print arXiv:1805.07165  
Di Paolo C, Nesti F and Villante FL (2018) MNRAS 475:5385  
Djorgovski S and Davis M (1987) ApJ 313:59  
Dodelson S and Widrow LM (1994) PRL 72:17  
Donato F, Gentile G, Salucci P et al (2009) MNRAS 397:1169  
Donato F, Gentile G, Salucci P (2004) MNRAS 353:17  
Dressler A, Lynden-Bell D, Burstein D et al (1987) ApJ 313:42  
Ellis G et al (2018) Found Phys 48:1226  
Ettori S and Fabian AC (2006) MNRAS 369:L42  
Evoli C, Salucci P, Lapi A, Danese L (2011) ApJ 743:45  
Faber SM and Gallagher JS (1979) ARAA 17:135  
Fabricant D, Rybicki G and Gorenstein P (1984) ApJ 286:186  
Freeman KC (1970) ApJ 160:811  
Freese K (2017) IJMPD 26:1730012  
Gammaldi V (2016) EPJ Web Conf 121:06003  
Gammaldi V (2015) PhD Thesis. UCM Madrid  
García-Bellido (2017) J Phys Conf Ser 840:012032  
Gentile G, Salucci P, Klein U, Vergani D and Kalberla P (2004) MNRAS 351:903  
Gentile G, Burkert A, Salucci P et al (2005) ApJ 634:145  
Genzel R, Schreiber NMF, Übler H et al (2017) Nature 543:397  
Graves GJ and Faber SM (2010) ApJ 717:803  
Gratier P, Braine J, Rodriguez-Fernandez NJ et al (2010) A&A 522:A3  
Green AM (2016) PRD 94:063530  
Gondolo P (2002) PRD 66:103513  
Grillo C, Gobat R, Lombardi M, and Rosati P (2009) A&A 501:461  
Gurovich S, McGaugh SS, Freeman KC, et al (2004) PASA 21:412  
Hessman FV (2017) MNRAS 469:1147  
Hyde JB and Bernardi M (2009) MNRAS 396:1171  
Hoekstra H and Jain B (2008) Annu Rev Nucl Part Sci 58:99  
Hui L, Ostriker JP, S Tremaine and E Witten (2017) PRD 95:043541  
Hudson MJ, Gillis BR, Coupon J et al (2015) MNRAS 447:298  
Kang S, Scopel S, Tomar G, and Yoon J.-H (2018) ArXiv e-print arXiv:1805.06113  
Karukes EV and Salucci P (2017) MNRAS 465:4703  
Karukes EV, Salucci P, and Gentile G (2015) A&A 578:A13  
Kaplinghat M, Linden T, and Yu H-B (2015) PRL 114:211303  
Kennedy R, Frenk C, Cole S, and Benson A (2014) MNRAS 442:2487  
Klypin A, Trujillo-Gomez S, and Primack J (2011) ApJ, 740:102  
Kolb, EW and Turner, MS (1990) The Early Universe, Addison Wesley, New York  
Kormendy J and Freeman KC (2004) In: Ryder SD et al (eds) Dark Matter in Galaxies (IAU S220), San Francisco, ASP, p 377  
Korsaga M, Carignan C, Amram P et al (2018) MNRAS 478:50  
Koushiappas SM and Loeb A (2017) PRL 119:041102  
Kregel M, van der Kruit PC, de Grijs R (2002) MNRAS 334:646  
Kusenko A (2009) Phys Rep 481:1

- Kuzio de Naray R, McGaugh SS and de Blok, WJG (2008) *ApJ* 676:920
- Jurić M and Ivezić Ž, Brooks A et al (2008) *ApJ* 673:864
- Jungman G, Kamionkowski, M Griest K (1996) *Phys Rep* 267:195
- Jorgensen I, Franx M, and Kjaergaard P (1996) *MNRAS* 280:167
- Impey C, Bothun G, and Malin D (1988) *ApJ* 330:634
- Lapi A, Salucci P and Danese L.(2018) *ApJ* 859:2
- Lelli F, McGaugh SS and Schombert JM (2016a) *ApJL* 816:L14
- Lelli F, McGaugh SS and Schombert JM (2016b) *AJ* 152:157
- Li B, Shapiro PR, Rindler-Daller T (2017) *PRD* 96:063505
- Lisanti M (2017) In: Polchinski J and Vieira P and DeWolfe, O (eds) *New Frontiers in Fields and Strings*. World Scientific, Singapore, p 399–446
- Magoulas C, Springob CM, Colless M et al (2012) *MNRAS* 427:245
- Maraston C (2013) In: Thomas D, Pasquali A, Ferreras I (eds) *The Intriguing Life of Massive Galaxies (IAU S295)* Cambridge, CUP, p 272
- Mamon, G and Lokas EL (2005) *MNRAS* 363:705
- Martinsson T, Verheijen M, Westfall K et al (2013) *A&A* 557:131
- Matteucci F (2012) *Chemical Evolution of Galaxies*. Berlin, Heidelberg, Springer
- McGaugh SS, Schombert JM, Bothun GD, de Blok WJG (2000) *ApJL* 533:L99
- McGaugh SS, (2005) *ApJ* 632:859
- McMillan PJ (2011) *MNRAS* 414:2446
- Moster BP, Somerville, RS, Maulbetsch C et al (2010) *ApJ* 710:903
- Müller O, Pawłowski MS, Jerjen T et al (2018) *Science* 359:534
- Munshi D, Valageas P, van Waerbeke L and Heavens A (2008) *Phys Rep* 462:67
- Naab T and Ostriker JP *ARAA* (2017) 55:59
- Navarro JF, Frenk CS and White SDM (1997) *ApJ* 490:493
- Nesti F and Salucci P (2013) *JCAP* 7,16
- Noordermeer E, van der Hulst JM, Sancisi R et al (2007) *MNRAS* 376:1513
- Oguri et al (2014) *MNRAS* 439 2494
- Oh S-H et al (2008) *AJ* 136:2761
- Oh S-H, Brook C, Governato F et al (2011) *AJ* 142:24
- Oh S-H, Hunter DA, Brinks E et al (2015) *AJ* 149:180
- Oman KA, Navarro JF, Fattahi A et al (2015) *MNRAS* 452:3650
- Honma, M, Nagayama, T, Ando, K, et al (2012) *PASJ* 64:136
- Palunas, P and Williams, TB (2000) *AJ* 120:2884
- Pascale R, Posti L, Nipoti C, Binney J (2018) *MNRAS* 480:927
- Pato M and Iocco F (2017) *SoftwareX* 6:54
- Persic M and Salucci P (1995) *ApJS*, 99:501
- Persic M, Salucci P and Stel F (1996) *MNRAS* 281:27
- Persic M and Salucci P (1990) *MNRAS* 245:577
- Persic M and Salucci P (1991) *ApJ* 368:60
- Planck Collaboration, Ade PAR, Aghanim N et al (2016) *A&A* 594:A13
- Plummer HC (1915) *MNRAS* 76:107
- Poci A, Cappellari M, McDermid RM (2017) *MNRAS* 467:1397
- Ponomareva AA, Verheijen MAW, Papastergis E et al (2018) *MNRAS* 474:4366
- Posacki S, Cappellari M, Treu T et al (2015) *MNRAS* 446:493
- Pulsoni C, Gerhard O, Arnaboldi M et al (2017) *A&A* 618:A94
- Ratnam C and Salucci P (2000) *NewA* 5:427
- Richards EE, van Zee L, Barnes KL et al (2015) *MNRAS* 449:3981
- Ringwald A (2012) *Phys Dark Univ* 1:116
- Roberts MS (1978) *AJ* 83:1026
- Roszkowski L, Sessolo EM, Trojanowski S (2017) *Rep Prog Phys* 81:066201
- Rubin VC, Ford WK Jr and Thonnard N (1980) *ApJ* 238:471
- Salucci P (2001) *MNRAS* 320, L1
- Salucci P, Nesti F, Gentile G, Frigerio Martins C (2010) *A&A* 523:83
- Salucci P, Frenk CS, Persic M (1993) *MNRAS* 262:392
- Salucci P and Burkert A (2000) *ApJL* 537:L9
- Salucci P, Lapi A, Tonini C, Gentile G, Yegorova I, Klein U (2007) *MNRAS* 378:41
- Salucci P, Yegorova IA, and Drory N (2008) *MNRAS* 388:159

- Salucci P, Wilkinson MI, Walker MG et al (2012) MNRAS 420:2034  
Salucci P and Turini N (2017) ArXiv e-print arXiv:1707.01059  
Schneider P (1996) MNRAS 283:837  
Serra P, Oosterloo T, Cappellari M, den Heijer M, Jozsa GIG (2016) MNRAS 460:1382  
Shankar F, Lapi A, Salucci P (2006) ApJ 643:14  
Shi X and Fuller GM (1999) PRL 82:2832  
Shi D et al (2017) ApJ 846:26  
Simon JD (2005) PhD Thesis  
Sofue Y (2017) PASJ 69:R1  
Sofue Y (2013) PASJ 65:118  
Somerville RS and Dave R (2015) ARAA 53:51  
Spano M, Marcelin M, Amram P et al (2008) MNRAS 383:297  
Spekkens K, Giovanelli R, and Haynes MP (2005) AJ 129:2119  
Spergel DN and Steinhardt PJ (2000) PRL 84:3760  
Steigman S and Turner MS (1985) Nucl Phys B 253:375  
Strauss MJ, Willick JA (1995) Phys Rept 261:271  
Strigari LE, Bullock JS, Kaplinghat M et al (2008) Nature 454:1096  
Strigari LE, Frenk CS, White SDM (2018) ApJ 860:56  
Thomas J, Saglia RP, Bender R et al (2011) MNRAS 415:545  
Tinsley BM (1981) MNRAS 194:63  
Tiret O, Salucci P, Bernardi M, Maraston C, Pforr J (2011) MNRAS 411:1435  
Toloba E, Lim S, Peng E et al (2018) ApJL 856:L31  
Tortora C, La Barbera F, Napolitano NR et al (2014) MNRAS 445:115  
Tortora C, Napolitano NR, Roy N et al (2018) MNRAS 473:969  
Treu T (2010) ARAA 48:87  
Tulin S, Yu H, Zurek KM (2013) PRD 87:115007  
Tulin S, Yu H (2018) Phys Rep 730:1–57  
Tully RB and Fisher JR (1977) A&A 54:661  
Turner MS (2018) Found Phys 48:1261  
van Albada TS, Bahcall JN, Begeman K et al (1985) ApJ 295:305  
van der Kruit PC and Searle L (1981) A&A 95:105  
van der Kruit PC (1988) A&A 192:117  
van der Kruit PC and Freeman KC (2011) ARAA 49:301–371  
van Dokkum PG, Romanowsky AJ, Abraham R et al (2015) ApJL 804:L26  
Verheijen MAW (2001) ApJ 563:694  
Viel M, Branchini E, Cen R et al (2005) MNRAS 360:1110  
Vogelsberger M, Genel S, Springel V et al (2014) Nature 509:177  
Vogt NP, Haynes MP, Herter T, Giovanelli R (2004a) AJ 127:3273  
Vogt NP, Haynes MP, Herter T, Giovanelli R (2004b) AJ 127:3325  
Walker MG, Mateo M, Olszewski EW (2009a) AJ 137:3100  
Walker MG, Mateo, M, Olszewski EW et al (2009b) ApJ 704:1274  
Walker M (2013). In: Oswalt TD and Gilmore G (eds) Planets, Stars and Stellar Systems  
5. Springer, Dordrecht, p 1039–1089  
Walker MG and Penarrubia J (2011) ApJ 742:20  
Wang J, Fu J, Aumer M et al (2014) MNRAS 441:2159  
Watkins LL, Evans NW, and An JH (2010) MNRAS 406:264  
Wechsler RH, Zentner AR, Bullock JS et al (2006) ApJ 652:71  
Wechsler RH and Tinker JL (2018) ARAA 56:435  
Weinberg S (1978) PRL 40:223  
Wolf J, Martinez GD, Bullock JS et al (2010) MNRAS 406:1220  
Xue XX et al (2008) ApJ 684:1143.  
Yegorova IA and Salucci P (2007) MNRAS 377:507  
Zaritsky D (2012) ISRN Astron Astrophys 2012:189625  
Zavala J, Vogelsberger M and Walker MG (2013) MNRAS 431, L20  
Zhao H (1996) MNRAS 278:488  
Zu Y and Mandelbaum R (2015) MNRAS 454:1161